OPPORTUNITES FOR THERMOELECTRIC ENERGY CONVERSION IN HYBRID VEHICLES

By

Christopher M. Jaworski

Advisors:

Dr. Yann G. Guezennec
Dr. Joseph P. Heremans
Dr. Gregory Washington
Dr. Giorgio Rizzoni

Submitted May 18, 2007

The Ohio State University
Department of Mechanical Engineering

Abstract

Due to the inefficiencies in automobiles, roughly two-thirds of the energy from the fuel is lost through braking, engine cooling, or exhaust gasses. The remaining third is used to drive the vehicle and power its accessories. Utilizing thermoelectric devices, it is possible to regain a portion of this lost thermal energy in the form of electrical power. Due to the relatively low efficiency of thermoelectrics, little analysis and design has been conducted concerning their usage in automobiles. Recently, developments in new thermoelectric materials show promise and could possibly demonstrate efficiency double that of commercially available materials. Analysis will begin with the development of a computer model to simulate different thermal energy management scenarios in a hybrid vehicle utilizing thermoelectrics. Based upon these results, a benchtop demonstration model will be constructed for validation with the ultimate goal of a working thermoelectric model in a hybrid vehicle.

Acknowledgments

I would like to thank my advisors, Dr. Heremans, Dr. Washington, Dr. Guezennec and Dr. Rizzoni for their continuous support and guidance throughout my research project. Drs. Washington and Heremans were kind enough to schedule weekly meetings with Leon and myself to discuss this project. Dr. Subramaniam deserves acknowledgement as he piqued my interest in thermoelectrics and energy conversion. Leon Headings has provided me with constant help and guidance as well. I would like to thank the College of Engineering for the internship I was awarded which allowed my pursuit of this project. Furthermore, Jim Shively, with his electronics knowledge, and Don Williams, with his machining expertise, provided greatly appreciated assistance. I would like to thank Randy Vezdoz and Charles Wiggermann for their ideas in designing the setup and solving problems that I encountered. Finally, I would to thank my family for their support throughout this project and during my years as an undergraduate student at Ohio State.

Table of Contents

List of Tables

List of Figures

Nomenclature

A	Area
α	Seebeck coefficient
c_p	Specific heat
G	TE geometry factor
h_c	Convective heat transfer coefficient
I	Current
I_{SC}	Short circuit current
κ	Thermal conductivity
K	Thermal conductance
L	Length
L_c	Characteristic Length
$\dot{m}$	Mass flow
n_{couple}	Number of couples in each Peltier module
η_f	Fin efficiency
ρ	Electrical resistivity
π	Peltier coefficient
P	Power
Q	Heat flow
R	Electrical resistance
R_{load}	Electrical load resistance
t	Fin thickness
T	Temperature
Θ	Temperature difference
V	Voltage
V_{OC}	Open circuit voltage
Z	Figure of merit
ZT	Dimensionless figure of merit

Introduction

Motivation

In a typical automobile today, approximately 65-85% of the fuel energy is lost to braking, heat loss, drive train friction, and other accessories [1]. A schematic depicting these losses is shown in Figure 1.

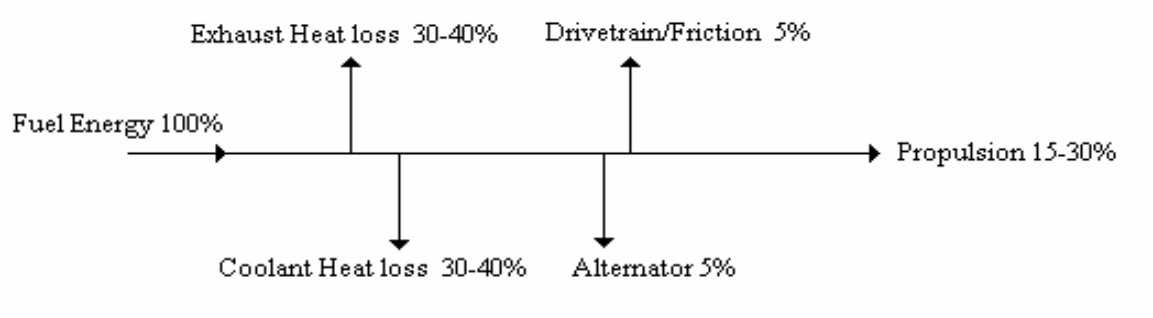

Figure 1 Automobile energy losses

The increasing cost and impending depletion of oil, along with state and federal government regulations requiring automotive vehicles to be more environmentally friendly, led to the creation of the electric-hybrid vehicle. These vehicles incorporate battery packs, electric motors, and regenerative braking to increase the efficiency of the engine. The motors provide power to the wheels while regenerative breaking is able to save a portion of the energy traditionally lost to frictional braking. These systems have achieved significant improvements in fuel economy. However, these hybrid vehicles ignore two other significant sources of energy loss: engine cooling and exhaust gas. Thermoelectric devices make it possible to regain a portion of this energy in the form of electrical power. Implementing thermoelectrics in hybrids presents unique design considerations. An advantage hybrids have is an extensive electric system that is already in place to utilize the electrical power that the thermoelectric devices generate. Generated electrical power could be used to charge the battery pack, and in turn, drive the motors.

However, in a hybrid electric vehicle, the amount of thermal energy flowing out the exhaust and radiator is lowered due the car's increased efficiency. Also, the internal combustion engine does not run continually, creating problems powering belt-driven accessories and maintaining interior cabin climate and catalytic converter temperature. Due to the effects of the internal combustion engine's running pattern, the demand for electrical power is increased in hybrids. If the energy recovered from the waste heat was sent to the battery pack, the alternator load could be removed from the engine providing an increase in efficiency of the vehicle.

Background

Thermoelectric Theory

Materials with thermoelectric properties are able to convert between electrical and thermal energy due to the Seebeck and Peltier Effects. The Seebeck Effect accounts for the electrical potential difference that arises due to a temperature difference across a junction of different materials. Materials have a Seebeck Coefficient which is defined as $\alpha = \frac{\Delta V}{\Delta T}$ and has units of V/K. Typical coefficients of materials used in thermoelectric modules range around $200 \mu V / K$. Figure 2 contains a diagram depicting how the Seebeck Effect works. The temperature difference creates a voltage across the material.

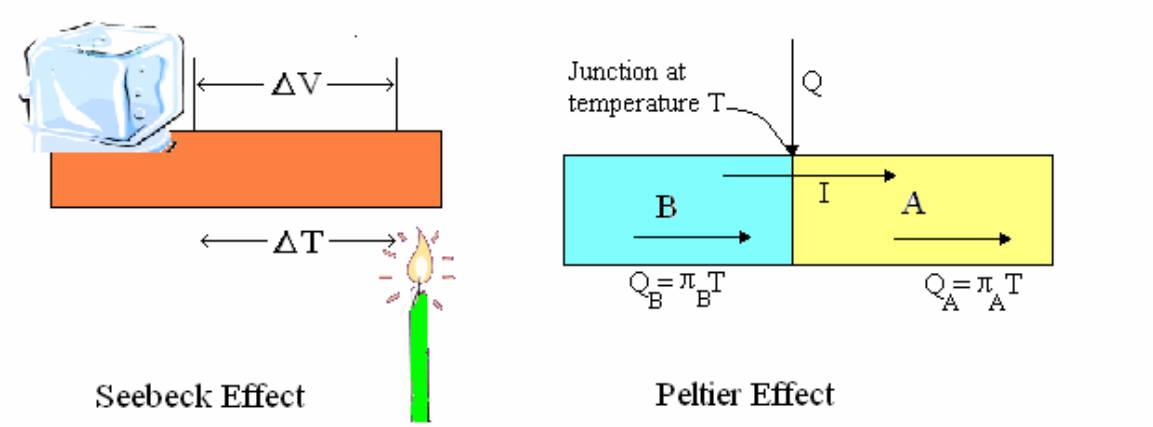

Figure 2 Seebeck Effect and Peltier Effect illustrations

The Peltier Effect is the reversible heat exchange that occurs when current flows through a junction of two different materials. The heat Q is emitted as current I flows from A to B. The Peltier coefficient is defined as: $\pi_{AB} = \frac{Q}{I}$. Furthermore, $\pi_{AB} = -\pi_{BA}$. When dealing with thermoelectrics, it is convenient to label $\pi_B I$ as the amount of heat flowing to the junction from material B due to the current flow towards the junction. Heat can be liberated or absorbed depending on the direction of the current. The Seebeck and Peltier effects are linked through the relation: $\pi_A = T\alpha_A$. These effects are distinct from Joule resistance heating. Because they operate due to junctions of dissimilar conductors, these two effects make thermoelectric devices unique in their ability to transfer thermal energy to electrical energy and back [2, 3].

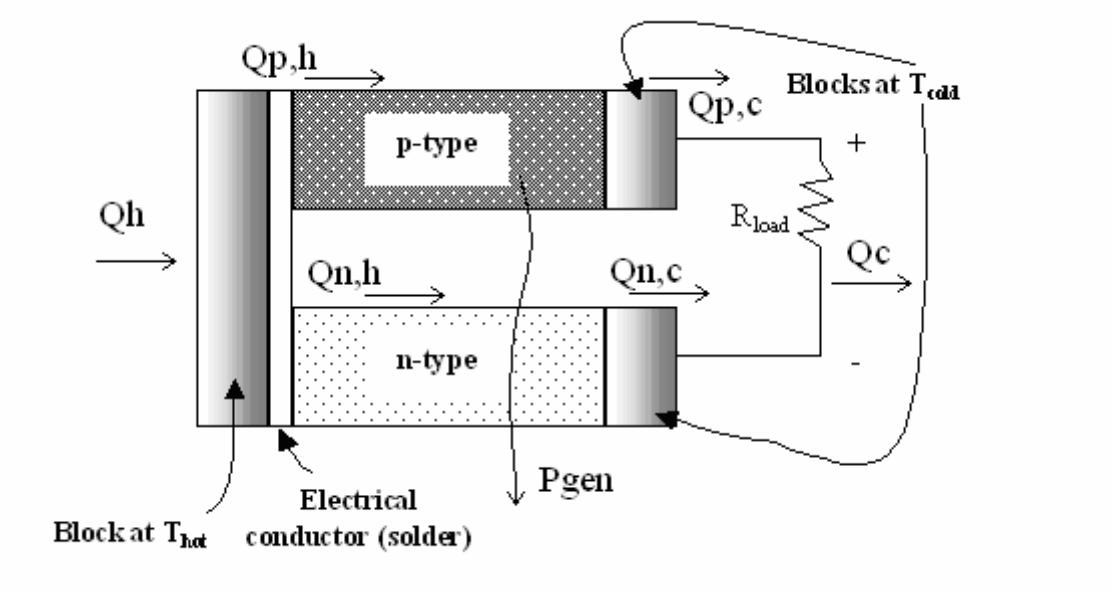

Figure 3 Schematic of one couple in a Peltier module [3]

Performing a heat analysis on the hot side of the couple shown in Figure 3 yields

$$Q_{total,h} = Q_{p,h} + Q_{n,h} = (T_h - T_c)\left[\frac{\lambda_p A_p}{L_p} + \frac{\lambda_n A_n}{L_n}\right] + (\alpha_p - \alpha_n)T_h I - \frac{I^2}{2}\left[\frac{\rho_p L_p}{A_p} + \frac{\rho_n L_n}{A_n}\right], \quad [3]$$

where A and L are the area and length of the legs, T_h and T_c are the temperatures of the hot and cold sides, I is the current passing through, ρ is the resistivity, λ is the thermal conductivity and α is the Seebeck coefficient. The first term is due to the thermal conductivity of the legs. Typically, one sets $K = \frac{\lambda A}{L}$.The second term arises from the Peltier effect at the hot junction. Finally, the third term results from the Ohmic heating which arises from current flow. For ease of use, $R = \frac{\rho L}{A}$. This terminology will be used in subsequent equations. Only half of the current travels to the hot side thus introducing the factor of -½ in the equation. A heat analysis of the cold side of the couple yields a similar equation with several key differences:

$$Q_{total,c} = Q_{p,c} + Q_{n,c} = (T_h - T_c)\left[K_p + K_n\right] + (\alpha_p - \alpha_n)T_c I + \frac{I^2}{2}\left[R_p + R_n\right]$$

First, the Peltier term is evaluated at the cold side temperature. Additionally, the resistive heat is added to this side. As the generated power will vary depending on the load resistance, R_L, it is useful to define $P=I^2R_L$. Now, the current is equal to the open circuit voltage of the couple divided by the source and load resistance:

$$I = \frac{V_{OC}}{R_L + R_S}.$$

Furthermore, using Seebeck's relation $\Delta V = \Delta\alpha \cdot \Delta T$, the open circuit voltage is defined as $V_{OC} = (\alpha_p - \alpha_n)(T_h - T_c)$. Combining these three equations together yields:

$$P = I^2 R_L = R_L\left(\frac{V_{OC}}{R_L + R_s}\right)^2 = \frac{(\alpha_p - \alpha_n)^2 \Delta T^2 R_L}{(R + R_L)^2}.$$

Through further development of these equations that will not be pursued here, it is found that the source resistance must equal the load resistance for maximum power generation [2]. This can be referred to as impedance matching of the source to the load. This fact produces the equation:

$$P_{\max} = \frac{(\alpha)^2 \Delta T^2}{4R_{load}} = \frac{V_{oc}^2}{4R_{load}}.$$

Finally, efficiency while operating at this maximum power can be written as:

$$\eta_{TE} = \frac{T_h - T_c}{\frac{4}{Z} - \frac{T_h - T_c}{2} + 2T_h}$$

Where Z is the Figure of merit evaluated at the average temperature of the couple [3].

The standard quantity used in evaluating the efficiency of thermoelectric materials is Z, the Figure of Merit. As Z increases, the performance of the thermoelectric material will increase. The Figure of Merit varies for a given thermoelectric material with temperature. As the Figure of Merit has units of K^{-1} (inverse of temperature), the quantity ZT is often used to evaluate thermoelectrics [2]. This quantity ZT is termed the dimensionless Figure of Merit. It is determined by multiplying the Figure of Merit at a given temperature by the temperature. Until recently, materials with only a ZT of approximately 1 existed. Recent developments have demonstrated materials with ZT in the area of 2 [4].

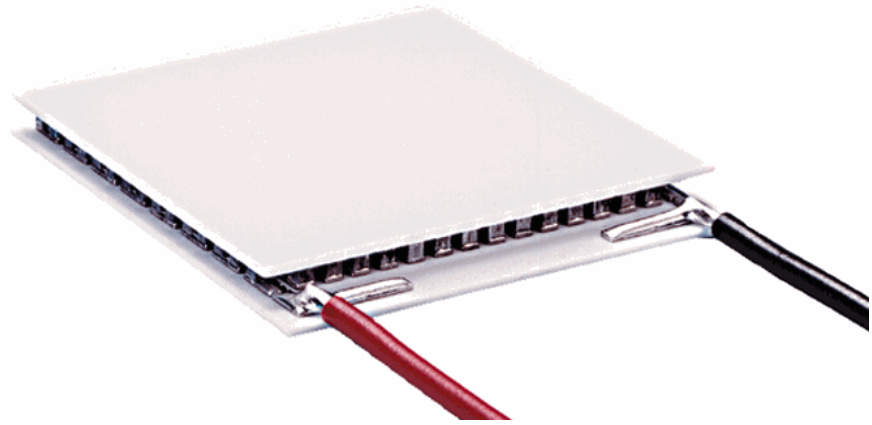

Figure 4 Typical Peltier module

Thermoelectric devices are a generic term for what is commercially available as a Peltier module. Peltier modules have three uses: cooling, heating and power generation. Heating and cooling require an electric current, while power generation requires a temperature gradient. Please reference Figure 4 for a photograph of a commercially available Peltier Module. A typical Peltier module sandwiches numerous sets of semiconductor legs, called couples, between two ceramic plates. Each couple consists of

a p-type and an n-type semiconductor, as shown in Figure 3. A typical module is composed of nominally one hundred of these couples electrically wired in series.

Previous Research

While the usage of thermoelectrics for waste heat recovery in automobiles has not been studied extensively due to thermoelectrics' historically low efficiencies, some experimental research has been completed. The amount of research has spiked in recent years due partly to the development of quantum well and superlatice thin-film thermoelectric materials with higher Figure of Merits.

A major portion of the research completed has been in using thermoelectrics on large diesel engines due to their high power output. Because these engines are larger, it is easier to transform enough thermal energy into electrical energy to make the thermoelectric generator viable. A team led by Bass studied waste heat sources available in diesel vehicles and concluded that an exhaust system thermoelectric generator would work best due to the higher ΔT available. They also studied different TE materials for use on an exhaust based heat exchanger including PbTe, SiGe, and Bi_2Te_3, and concluded that Bi_2Te_3(Bismuth Telluride) offered the best performance despite its limited hot side temperature [5]. Using 72 Bi_2Te_3 thermoelectric modules, Bass et al. constructed a thermoelectric generator using the exhaust of a 14 liter 350 hp Cummings engine and succeeded in generating 1kW of electricity at maximum load conditions [6].

Other researchers have focused on implementing a thermoelectric generator in vehicles with gasoline engines. Ikoma, et al. designed and constructed an exhaust based thermoelectric generator. Utilizing SiGe modules, the generator produced 35.6 watts of electric power. This fell short of expectations, and the team concluded more research

would need to be completed to improve thermoelectric material properties and heat transfer [7]. Hendricks and Lustbader researched the use of thermoelectrics to extract heat from vehicle exhaust using an extensive computer program based in a MATLAB/Simulink environment. From their modeling, up to 900 watts of recoverable electrical power has been predicted for a light-duty passenger vehicle. In their research, they had not focused on the actual design of a generator in a vehicle and identified areas such as electrical and thermal interface design, lowering system costs, and verifying their predictions in a physical experiment as the areas to focus on next. [8]

Due to the lower ΔT between the coolant and ambient air available in the radiator, the radiator has not been examined as extensively. In his dissertation, Crane created extensive computer models of a thermoelectric generator recovering waste heat in the radiator [9]. The modeling included both transient and steady state cases of a GM Chevrolet Suburban with a 5.3L V8 engine. Unlike previous attempts, Crane attempted to optimize the actual heat recovery and thermoelectric design in accordance with automotive constraints including: increased drag from a larger radiator, additional cost, and increased weight [9]. He was unable to design a thermoelectric radiator that would produce enough power to displace the alternator but concluded that a smaller alternator could be used in junction with the thermoelectric radiator.

Direction

In approaching the problem of waste heat recovery, the team has decided to exclusively design for a hybrid-electric vehicle. We have chosen this because the hybrid-electric vehicle will be able to use the electricity generated not only to power accessories but possibly the wheels. Initially, the team will be looking at a higher-level evaluation of

thermal energy management strategies. Instead of optimizing the design at one point, we will be evaluating a variety of system configurations and the vehicle's thermal systems as a whole. Once the best overall configuration is selected, the team will begin to optimize the design of individual components.

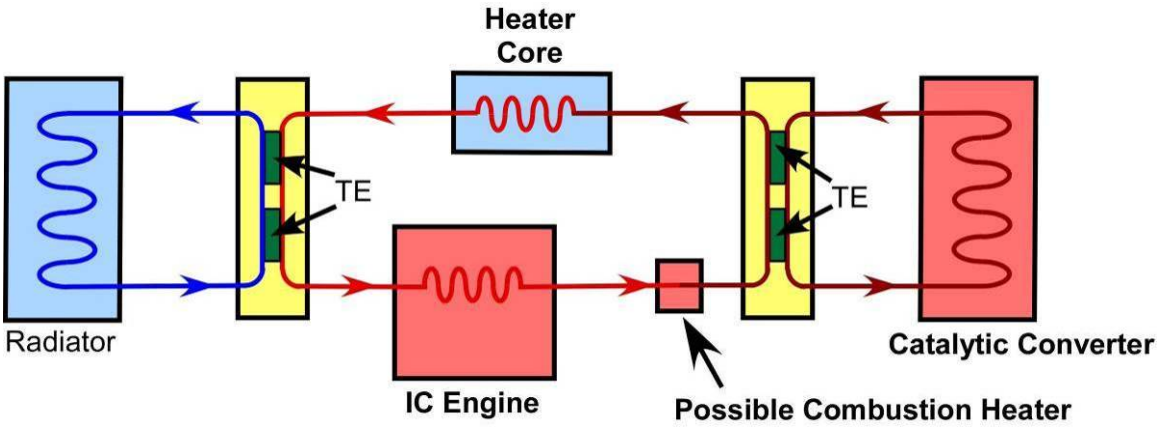

Figure 5 Theoretical layout for the positioning of key components [10]

In the configuration depicted in Figure 5, three fluid loops create temperature differences across the thermoelectric modules, allowing them to generate power. All of the heat must be dissipated through the radiator. This design consists of four heat exchangers: two are thermoelectric liquid to liquid; the other two are conventional gas to liquid.

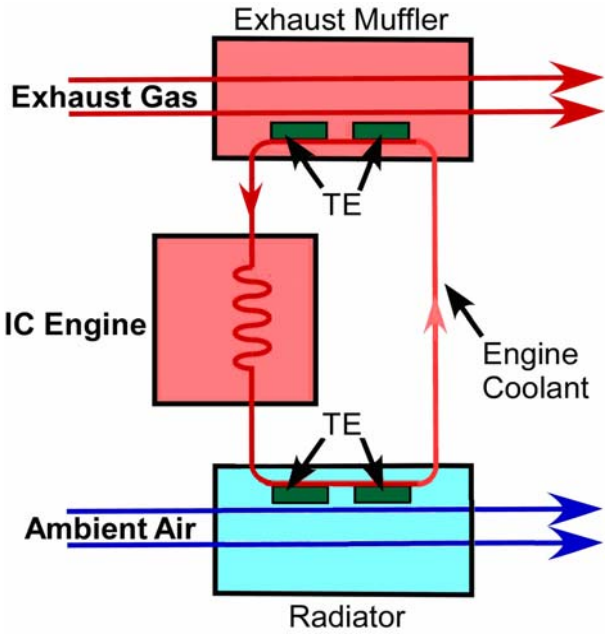

Figure 6 Theoretical thermal management scenario [10].

The layout shown in Figure 6 takes advantage of the very high exhaust gas temperatures and low ambient air temperatures to create temperature differences across the thermoelectrics. It consists of two air to liquid thermoelectric heat exchangers.

Two PhD. candidates, Leon Headings and Vincenzo Marano, have developed a Simulink computer model detailing the thermal energy transfers in a hybrid electric vehicle. Data from the Volkswagen TDI 1.9 L engine will be used in the model. Simulations with different hardware configurations including heat exchanger and material efficiencies, masses, fluid loops and other factors will be modeled and subsequently ranked on their performance in areas such as efficiency and total power generated. Utilizing the resources of Ohio State's Center for Automotive Research, the team will construct a small model of the chosen design for validation purposes. This benchtop experiment will be will be used to evaluate both liquid-to-liquid and liquid to air thermoelectric heat exchangers. In the experiment, data will be recorded for both

radiator (hot liquid to cold air) and exhaust (hot air to cold liquid) heat exchangers. The exhaust heat exchanger will be liquid cooled.

Physical Model

The first design that was constructed for the physical model allows the testing of both exhaust and radiator systems. The system was setup to allow heating of the fluid on either side of the heat exchanger. To simulate the exhaust system in an automobile, the air heater will be turned on and the liquid side will provide the cooling. For the radiator system, a cartridge heater will heat the liquid. Compressed air flowing through the heat exchanger will provide the cooling.

Configuration

Liquid Loop

As can be seen in Figure 7, the fluid starts its loop at the centrifugal pump. The liquid then passes through the throttling valve and then the electric water heater. At the exit of the heater, the temperature of the fluid is recorded. The flow proceeds through the liquid side of the thermoelectric heat exchanger. After exiting the heat exchanger, the temperature is measured again. Next the fluid mixture passes through the radiator for cooling. Variable speed electric fans were installed on the radiator to provide additional controllable cooling. The fluid finishes its loop by passing through the flowmeter. A fluid reservoir is positioned between the flowmeter and the pump to maintain proper fluid levels and remove air from the system.

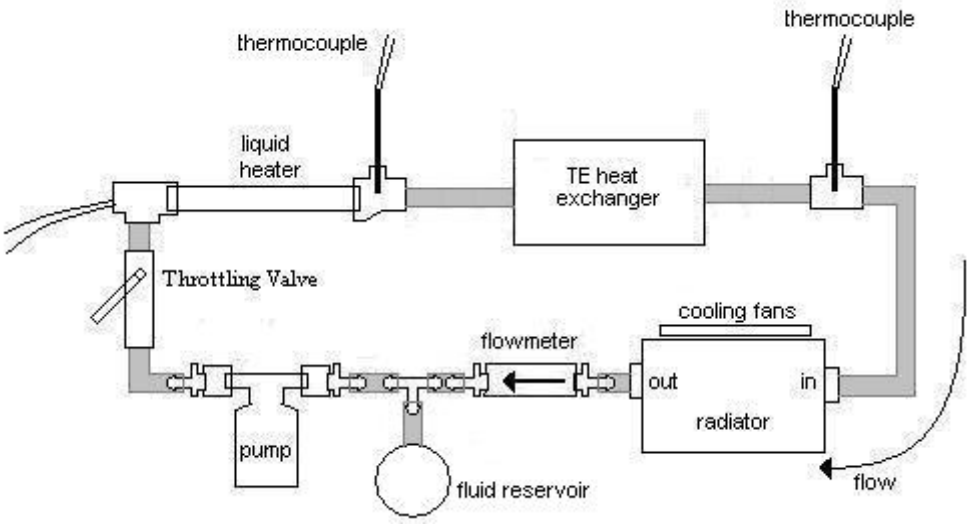

Figure 7 Schematic of liquid side of physical setup

Air Loop

Referring to Figure 8, compressed air first flows through the flowmeter at a chosen rate. It then passes through an air process heater. The temperature is recorded at the outlet and the air then flows into the thermoelectric heat exchanger. After exiting, the temperature is measured using a thermocouple. Finally, the air exits out a muffler that was installed in order to ensure sufficient back pressure.

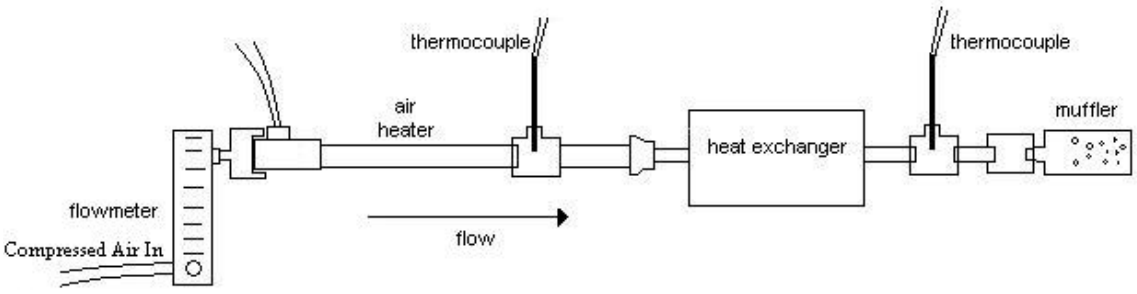

Figure 8 Schematic for air side loop

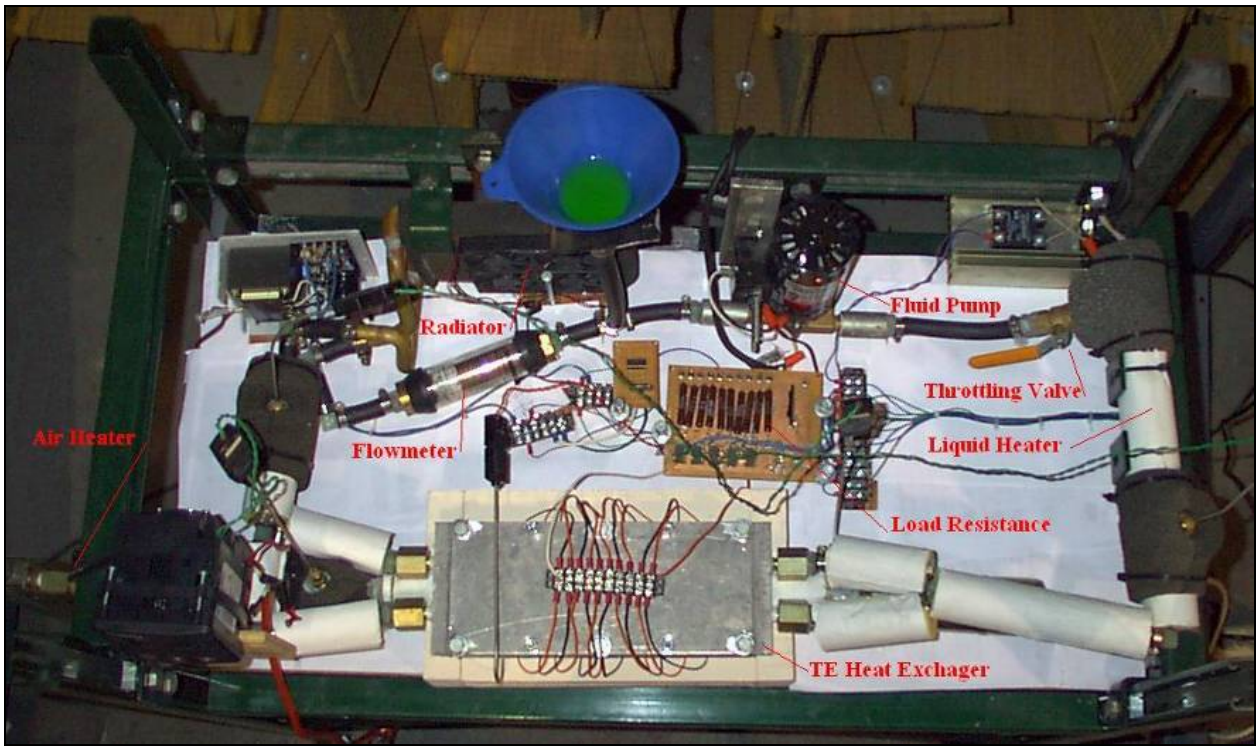

Figure 9 Photograph of experimental setup

Figure 9 is an image of the constructed experiment with labels for easier viewing.

Individual Components

A 1kW cartridge heater is used in the liquid loop. This will provide a 10 ºC increase at 0.42 GPM or a 2.5 ºC increase at 1.68 GPM of a 50/50 water ethylene glycol mix. From these numbers, a 1/25 hp high temperature bronze centrifugal pump with an AC motor was selected. A 750 W air process heater was chosen to heat the air. The maximum temperature that this heater can reach is 540 ºC. As a calculation used for sizing purposes, it can heat 2.8 SCFM air from 25 ºC to 450 ºC. 450 ºC was chosen as a nominal temperature based on results from the theoretical Simulink model. The model is approximately a 1:30 scale down of a 1.9 L TDI engine.

Flow regulators and flowmeters were installed into the fluid loops. Compressed air is passed through a rotameter, which is able to both control and measure the flow.

The model selected can pass 0- 6 2/3 standard cubic feet per minute (188 liters per minute). A throttling valve was selected to control the liquid flow. The flow rate is measured by a variable area flow meter that has a range of 0-2 gallons per minute (7.6 liters per minute).

Temperature measurements are taken at the inlets and outlets of the heat exchanger on both the liquid and air side. Ungrounded Type J thermocouples are used in the liquid loop and exposed Type J thermocouples are used in the exhaust loop. Another thermocouple was placed in the heat exchanger to ensure that the temperature of the heat exchanger would not exceed that of the maximum value allowed by the thermoelectric modules. The output voltages are fed into AD594 chips that amplify and provide cold junction compensation to the thermocouple voltages. The thermocouple that measures the output of the air heater is fed directly into a PI controller as well as an AD594 chip. This controller will regulate the output temperature of the fluid at the exit of an electric heater as set by the user. Fiberglass pipe insulation was placed around the tubes and hoses that were located between the temperature measurements on each side and on the heaters. The female tees were also covered with cellular glass insulation.

A method of removing the heat added to the liquid loop during exhaust testing is needed. The chosen method was the addition of a radiator into the loop. The radiator is a heater core taken from a Dodge Stealth. Four 12VDC electronic cooling fans measuring 40mm x 40mm were mounted on one side of the heater core to simulate an actual vehicle radiator. The fans will be controlled by a solid-state relay through a pulse width modulated signal from a Texas Instruments TL494 chip. A voltage sent from the data acquisition board controls this chip's output. The voltage will be controlled by the

temperature of the liquid at the inlet of the heat exchanger. If the fluid temperature is too high then the fans will speed up. Likewise, if the temperature is too low, the fans will slow down, thus allowing the fluid to heat up.

The connectors on the liquid loop are barbed polypropylene fittings that employ a worm clamp on the barb side to ensure leak free operation. To seal the threaded side, a RTV silicone gasket maker was applied to the threads before assembly. This successfully prevented leaks. This sealant was not necessary for any metal-to-metal pipe thread connections. Teflon tape was sufficient to prevent leaks for the all metal connections.

Electrical Load Resistance

Another requirement of the Peltier modules is that the electrical load resistance must be set equal to the modules' internal resistance for maximum power output. However, the internal resistance will change during each trial and between trials when different flow rates and temperatures are used. Therefore, the load resistance has to be variable. To satisfy these requirements, ten 10-Watt resistors were installed in parallel in the circuit. Each resistor had its own switch, thereby allowing the resistors to be switched on and off in different combinations. Roughly 1000 different resistances ranging from 1.5 ohms to 70 ohms are available. About 600 of the resistances range from 1.5 ohms to 7 ohms. This is the region of resistance that the internal impedance of the thermoelectric modules are calculated to be closest to. Each thermoelectric module has a nominal internal impedance of 3 ohms at the temperatures that will be reached. The modules can be set up electrically in several different configurations. Proposed setups are: all parallel, all series, and two parallel sets of five modules connected in series. Other configurations can be implemented.

Thermoelectric Modules

Due to its availability, cost, and operating temperature, Bi_2Te_3 thermoelectrics were chosen for this experiment. As concluded by Bass, its properties are well suited for waste heat recovery for both engine coolant and exhaust loops [5]. The TE module used in this study is the MELCOR HT6-12-40 (n_couple=127 and G=0.121 cm). The main properties, as reported by the manufacturer, are shown in Table 1. G is the ratio of Area / Length. The thermoelectric modules have a maximum hot side temperature of 225 ºC.

Table 1 Essential Properties for Thermoelectric Modules

T [K]	α [10^{-4}V/K]	ρ [10^{-3} Ω-cm]	κ [10^{-2} W/cm·K]	Z [10^{-3} 1/K]
273	1.94	0.92	1.61	2.54
300	2.02	1.01	1.51	2.68
325	2.07	1.16	1.53	2.44
350	2.10	1.28	1.55	2.22
375	2.00	1.37	1.58	1.88
400	1.96	1.48	1.63	1.59
425	1.90	1.58	1.73	1.32
450	1.86	1.68	1.88	1.06
475	1.79	1.76	2.09	0.87

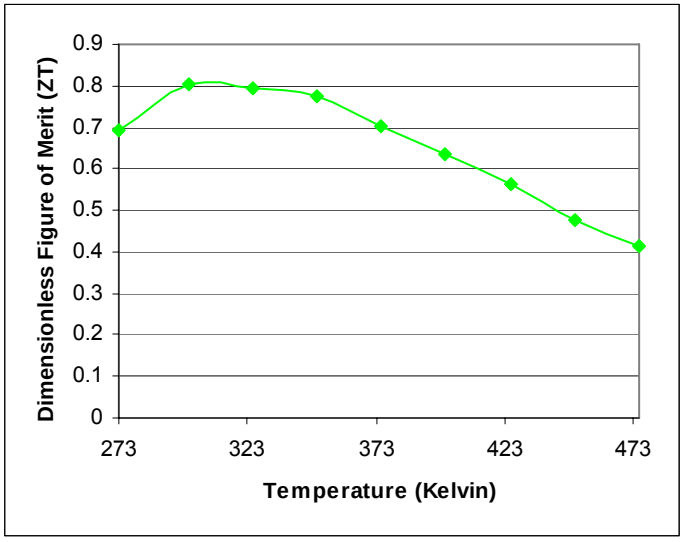

Figure 10 ZT for TE modules over temperature

Figure 10 displays the dimensionless Figure of Merit (ZT) over temperature. As can be seen, the Bismuth Telluride modules have a maximum ZT of 0.8 at 300 K. For each module overall electrical and thermal characteristics are given by the following equations:

$$V_{oc} = n_{couple} \times 2 \times \alpha \times \Delta T$$
$$K_{\mathrm{mod}} = n_{couple} \times 2 \times \kappa \times G$$
$$R_{\mathrm{mod}} = \frac{n_{couple} \times 2 \times \rho}{G}$$

[2]. V_{oc} is the open circuit voltage that is developed across the module, K_{mod} is the total thermal conductivity of the module and R_{mod} is the internal resistance of the module due to the resistivity of the p-type and n-type semiconductors. At 400K, the internal resistance of a module is 3.1 ohms and the thermal conductivity is 0.5 W/K. This does not include the resistance due to the solder that was used in the modules or thermal and electrical contact resistances, which are currently unknown. ΔT is the difference between the hot and cold sides of the Peltier module. From $\wp = I^2R_{load} = IV$, the current equals the open circuit voltage divided by the total summed resistance:

$$I = \frac{V_{oc}}{R_{\mathrm{mod}} + R_{load}}$$

The thermal heat flows entering and exiting the modules are given by the following equations, where Q_c represents the heat leaving the cold side and Q_h represents the heat entering the hot side. In order to maximize power, R_{load} is set equal to R_{mod}, [2], yielding:

$$Q_h = K_{\mathrm{mod}}\Delta T + n_{couple} 2\alpha T_h I - \frac{1}{2} I^2 R_{load}$$

$$Q_c = K_{\mathrm{mod}}\Delta T + n_{couple} 2\alpha T_c I + \frac{1}{2} I^2 R_{load}$$

Typically, the first term, thermal conductivity, results in seventy percent of the heat flux. The Seebeck and Peltier effects account for twenty-five percent, with the Ohmic resistance yielding the last five percent. Actual generated power for the combined setup is determined as a function of current and load resistance:

$$P_{gen} = I^2 R_{load} = \frac{V^2}{R_{load}}$$

Defining thermal efficiency as the ratio between electrical power out and the heat entering the hot side yields:

$$\eta_{TE} = \frac{P_{gen}}{Q_h}$$

When the maximum power approach is chosen, thermoelectric efficiency can be written as:

$$\eta_{TE} = \frac{T_h - T_c}{\frac{4}{Z} - \frac{T_h - T_c}{2} + 2T_h}$$

Heat Exchanger

Once the fluid flow rates and heaters were chosen, the dimensions for the heat exchanger were calculated. The heat exchanger was constructed out of aluminum plates. The exact material properties are unknown. The dimensions of the ten TE modules, which measure 40 x 43 mm each, constricted its length and width. This set the finned area of the base to be 86 x 200 mm. The height of the heat exchanger was also constrained to be within reason while still providing adequate heat transfer. Shown below in Figure 11 is a schematic of the heat exchanger. For this configuration, air is heated to temperatures simulating that of an exhaust in an automobile. The liquid is a

50/50 water ethylene glycol mixture that provides the cooling. Each side of the heat exchanger has six screws that secure the lids to the machined blocks. Four bolts are utilized to secure the contraption together, thus ensuring ample surface pressure on the thermoelectric modules. As can be seen, the thermoelectric modules are sandwiched between the two aluminum blocks. To facilitate heat transfer, OMEGABOND Thermal Grease was used on both sides of the Peltier modules. It has a maximum working temperature of 225 ºC. Calcium silicate insulation blocks were machined and assembled to form a cage around the heat exchanger to help stem heat loss. The blocks measured 1.5 inches thick. Fiberglass insulation was placed between the aluminum blocks of the heat exchanger where the modules were not present in order to reduce heat losses through radiation. Recommendations from the manufacturer for maximum heat transfer require the surface pressure on the modules to be between 150 and 300 psi.

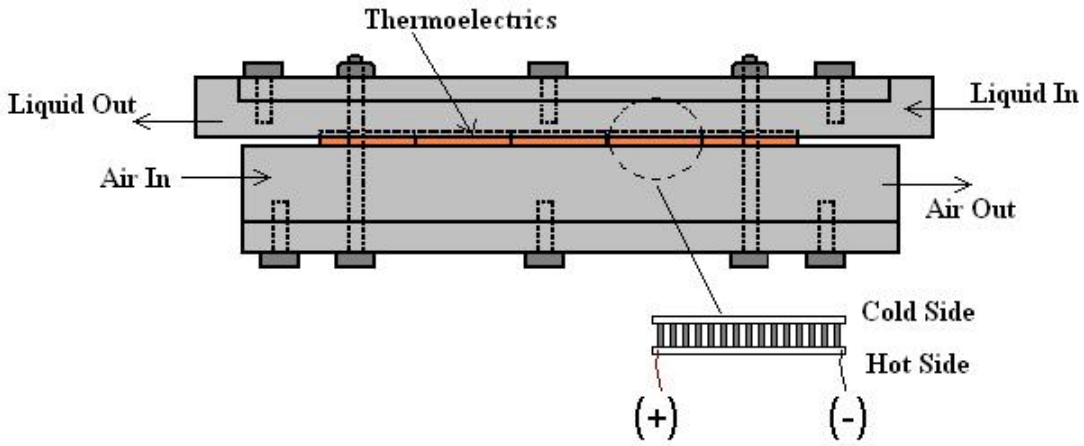

Figure 11 Schematic of heat exchanger layout

First Design of Thermoelectric Heat Exchanger

A simple design for the heat exchanger was chosen initially. Rows were machined into an aluminum block, thus forming fins. Please see Figure 13 for a

photograph of the uncapped liquid side of the exchanger. Two inlets and outlets were drilled to ensure adequate wetting of the entire exchanger by the water-ethylene glycol mixture. Both the air and liquid sides have the same geometry, just different dimensions.

The heat transfer through each side of the heat exchanger was calculated using standard fin equations, as can be found in any basic Heat Transfer textbook [11] and by Lee in his calculations for finned exhaust heat exchangers [12]. It is first convenient to define fin efficiency:

$$\eta_f = \frac{\tanh(mL_c)}{mL_c}$$

Where L_c is the effective length:

$$L_c = L + \frac{t}{2}$$

and m is defined as:

$$m = \sqrt{\frac{h_c P}{kA_c}}$$

P is the perimeter of the fin, h_c is the convective heat transfer coefficient of the liquid, k is the thermal conductivity for the base material, and A_c is the cross sectional area of the fin. L is defined as the length of the fin and t is the thickness. Furthermore, heat transfer through the fin can be calculated using $Q = (N \cdot \eta_f \cdot A_f + \cdot A_b) h_c \cdot \theta$, where Θ is the temperature difference between the fluid and the base, N is the number of fins, A_f and A_b are the areas of the fin and base, respectively. Please reference Figure 12 for a visual explanation of the previously discussed parameters and variables.

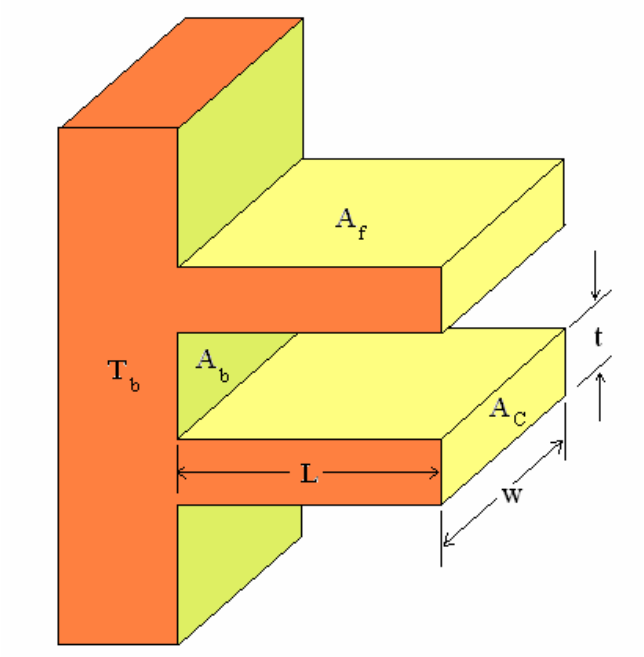

Figure 12 Explanation of parameters for heat exchanger calculation

Figure 13 Photograph of liquid side heat exchanger before installation.

Computer Aided Design

Matlab was used to determine the critical dimensions of the heat exchanger, including the number of fins and their width. Several scripts were written in order to make the design simpler. Initially, a script was written to calculate the heat flow through

the sides of the heat exchanger. Calculations were performed first for the liquid side. Initially, the height was set arbitrarily to 0.0095 m. With the width of the slots constrained to .0074 m (3/16") for ease of machining, Matlab was used to calculate the number of fins that would provide the best heat transfer. The width of the fins, Δ, was directly related to the number of fins by the relationship: $\Delta = \frac{(.095-(N+1)*(.0074)}{N}$. Also, as the fluid moves through the heat exchanger, its temperature drops. To account for this, the script was modified accordingly. The heat exchanger was divided into 'n' parts. The total heat flow from the heat exchanger was calculated. This was then divided by 'n' to give the heat flow for the first part, labeled 'k'. Dividing the heat flux by the mass flow rate and the specific heat yielded the temperature drop for the fluid in the first section. At the second section, 'k+1', the script ran again, but this time at the new starting temperature. Again, the temperature drop for 'k+1' section was calculated. This continued until the script ran n times. In addition, the temperature of the base of the heat exchanger will also drop through the heat exchanger. To account for this, the temperature of the base was reduced by 20 percent of the temperature drop of the fluid for each section. As can be seen, the heat flow is negative because heat is flowing into the liquid from the heat exchanger. These calculations are performed with a fluid entrance temperature of 89 ºC and an initial base temperature of 97 ºC. The convective heat transfer coefficient is assumed to be 2500 W/m^2*K and the thermal conductivity for aluminum 209 W/m*K. The plot in Figure 14 shows the results:

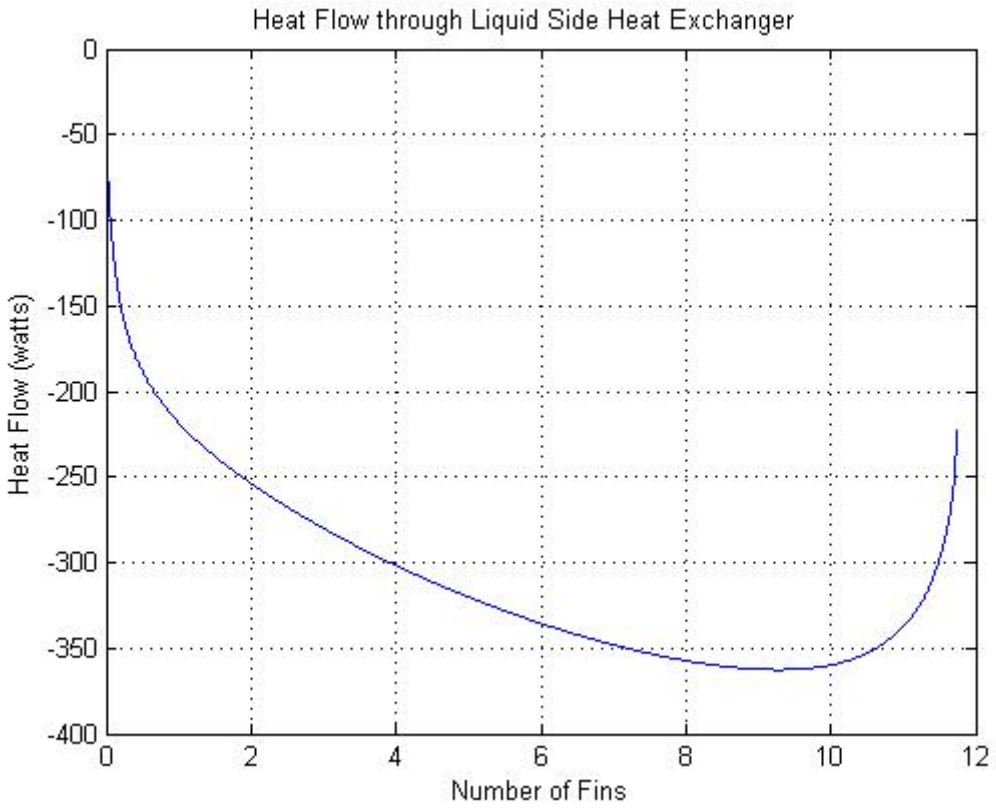

Figure 14 Relation of the heat flow through the liquid side of the heat exchanger and the number of fins that the heat exchanger has.

As can be seen, the plot includes numbers of fins which are less than one and in between 10 and 12. The calculation used a step size of .01 number of fins to provide a smoother curve. As the number of fins increases from zero to eight, the heat transfer from the increase in the number of fins outweighs the heat transfer lost due to the decrease in fin width. From around eight and nine fins onward, the decrease in heat transfer due to the smaller fin width outweighs the increase due to more fins. From this plot, nine fins were chosen for the heat exchanger.

Once the number, width, and spacing of the fins had been determined, the height was calculated. Again, a Matlab script was written and used to determine the best height of the fins. Initially the heat transfer was calculated for fin height ranging from 0-.05

meter (0-2in). This is shown in the top figure in Figure 15. As can be seen, the increase in the magnitude of heat flow decreases dramatically between .01-.02 m (.4 -.8 in). Therefore, the script was run again with the height of the fins ranging from 0-.02m. From the plot in Figure 16, it is seen that a height of .009 m (3/8") would provide roughly 360 watts of heat transfer, which is adequate.

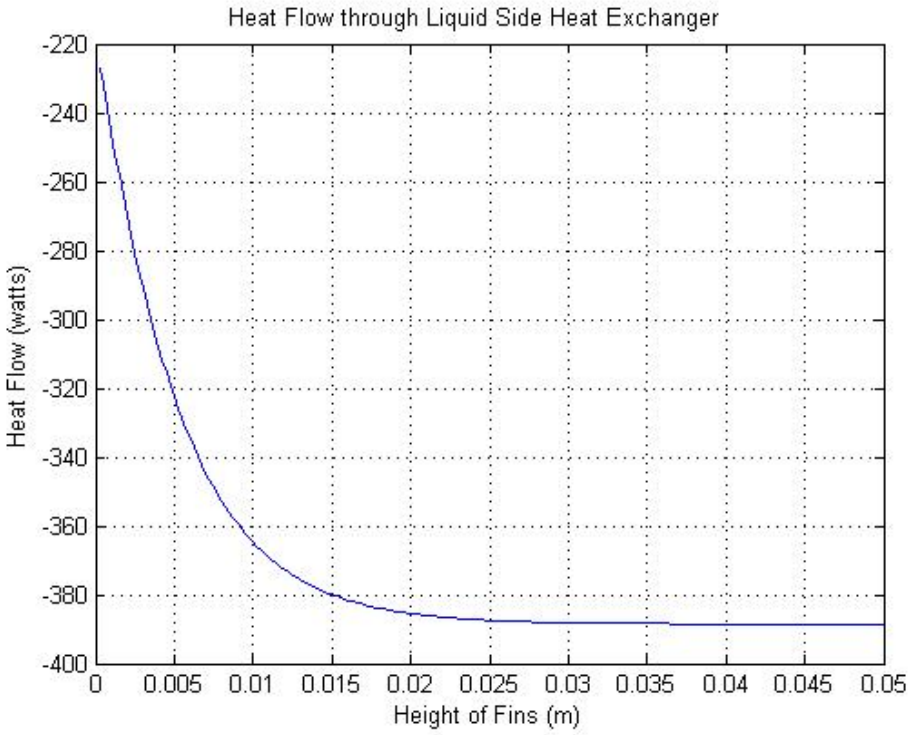

Figure 15 Heat flow through liquid side exchanger for 0-0.05 m fin height

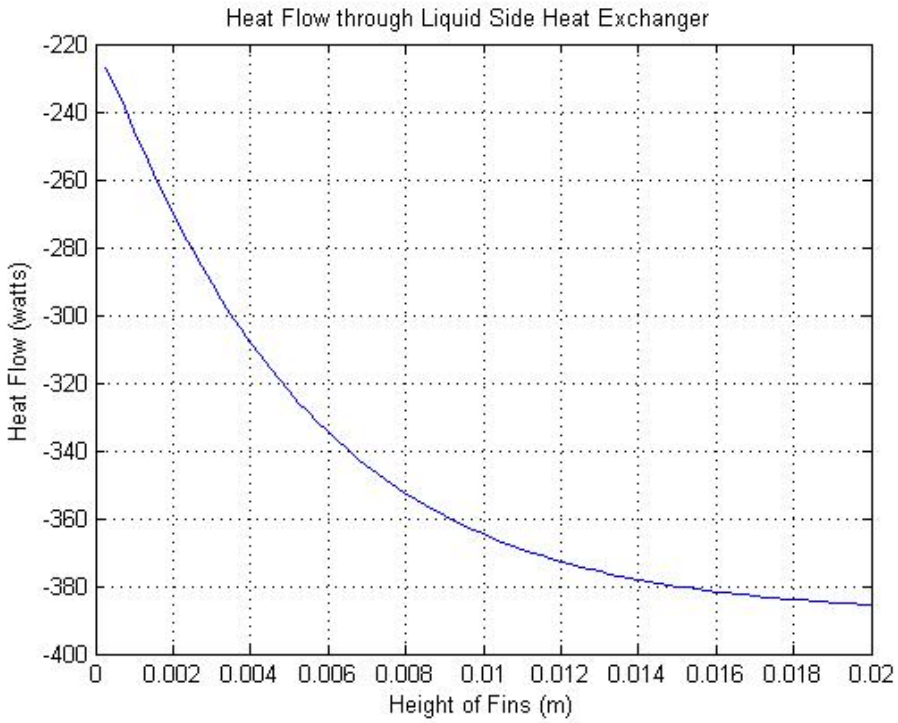

Figure 16 Heat flow through liquid side exchanger for 0-0.02m fin height

Air Side

The same basic scripts were used to model the air side of the heat exchanger. The only differences were the changes in the convective heat flow coefficient and temperatures of the liquid. These calculations are performed with a fluid entrance temperature of 450ºC and an initial base temperature of 200 ºC. The convective heat transfer coefficient is assumed to be 40 W/m^2*K and the thermal conductivity for aluminum is assumed to be 209 W/m*K. The first script to run calculated the heat flow for the air side based upon the height of the fins. The following plots in Figure 17 and Figure 18 show the results. Again, after the first script was run, the range of the height was narrowed from 0-0.2 m to 0- 0.05m. From this second plot, it is seen that a height of .0222m (.875 in) has adequate heat transfer that is in the range of the liquid heat exchanger.

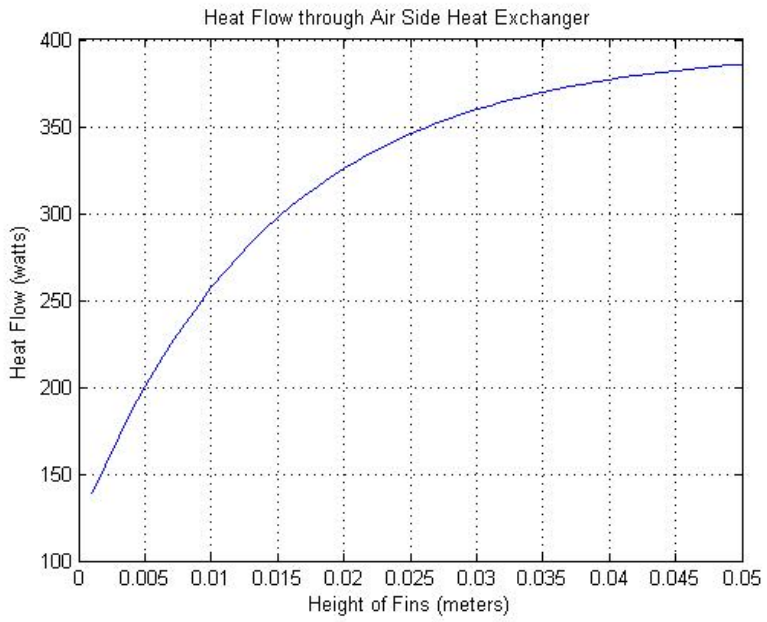

Figure 17 Heat flow through the air side of the heat exchanger for 0-0.05 m fin height.

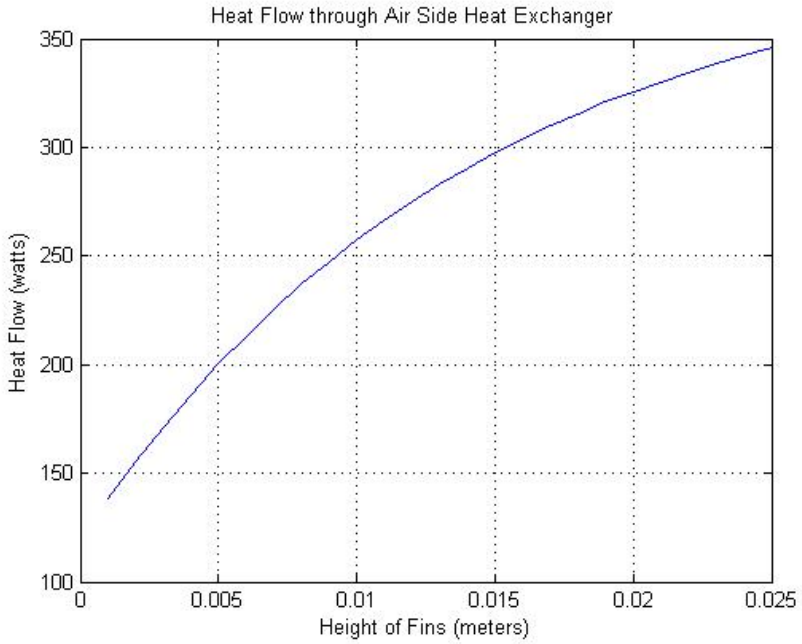

Figure 18 Heat flow through the air side of the heat exchanger for 0-0.02 m fin height.

To calculate the number of fins and their optimum width, the script that was created in Matlab for the liquid side was modified and run. The height was set at .0222 m (.875 in). The plot in Figure 19 shows the results:

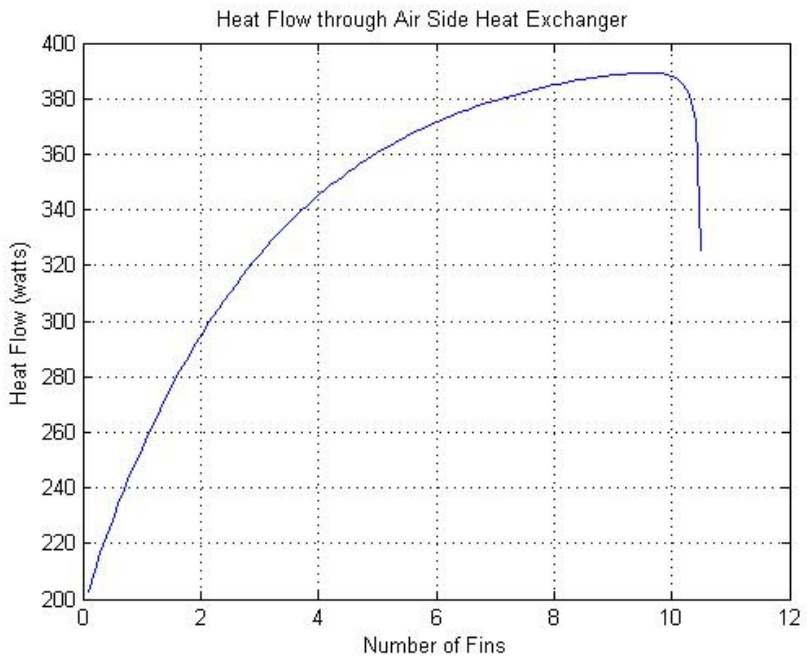

Figure 19 Relation of the heat flow through the air side of the heat exchanger and the number of fins that the heat exchanger has.

From Figure 19, 9 fins were chosen with each having a width of 5.3 mm. Using the aforementioned numbers, the aluminum blocks were machined using a mill and then assembled together. A high temperature RTV gasket sealant was used to prevent leakage on the liquid side.

Computer Simulation

In order to run the experiment, a data acquisition board and software was required. dSPACE was chosen as the setup to use in this experiment. It is able to interact with the Simulink software present in Matlab. The user initially sets up the simulation in Simulink and then imports it into the dSPACE system.

Figure 20 shows the Simulink block diagram for the hot air (exhaust) test. It contains five input and one output voltages. These signals are the temperatures and the

inlets and outlets of the heat exchanger as well as a surface measurement temperature of the heat exchanger. The output voltage is a signal that controls the fan speed.

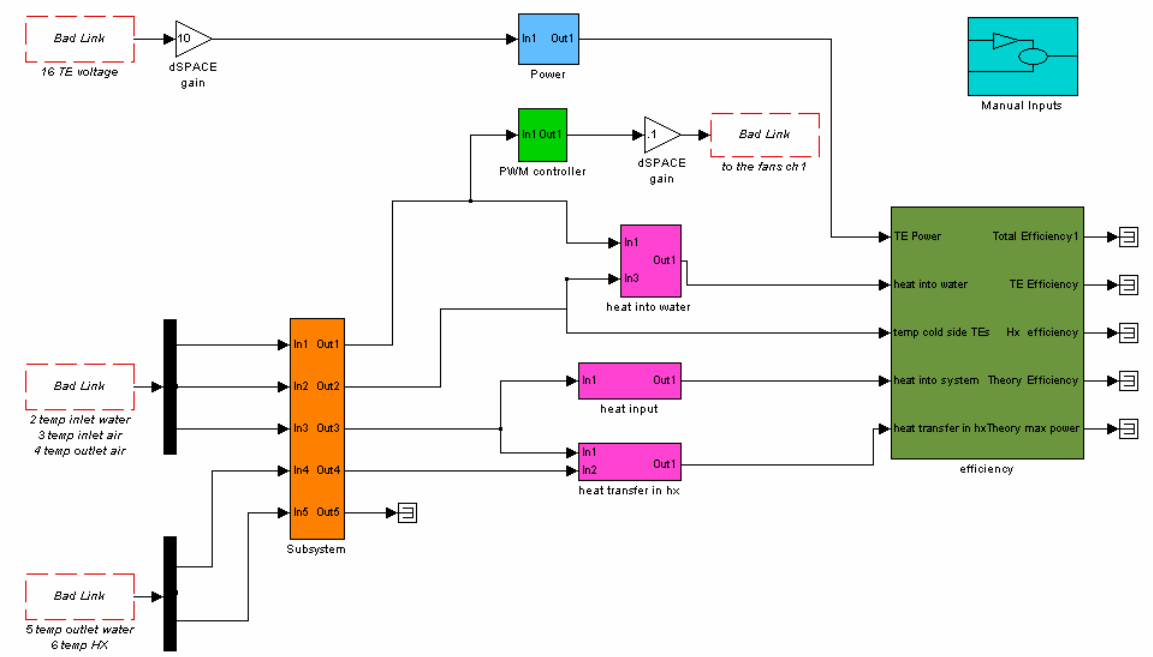

Figure 20 Example Simulink control system

Components Relevant to All Tests

Using Figure 20 as a guide, it can be seen that it contains several colored boxes. Except for the box at the top right, which is user defined inputs to the system, each contains a subsystem that is masked by the box. The box in the upper right hand corner masks the user inputs into the system. These consist of the liquid flow rate in gallons per minute, air flow rate in standard cubic feet per hour, ambient temperature in degrees Celsius, the load resistance in Ohms, V_{OC}, I_{SC}, and the desired temperature of the liquid loop. This box converts the volumetric flow rates into mass flow rates with the equations:

$$\dot{m} = [x]\frac{gallons}{minute} \bullet \frac{1minute}{60\,\mathrm{sec}onds} \bullet \frac{0.003785m^3}{1gallon} \bullet \frac{1056kg}{m^3} \bullet \frac{1000g}{1kg} = [x] \bullet 66.6\frac{g}{s} \text{ (Liquid)}$$

$$\dot{m} = [\mathrm{x}]\frac{\mathrm{ft}^3}{\mathrm{hour}} \bullet \frac{1\,\mathrm{hour}}{3600\,\mathrm{seconds}} \bullet \frac{.0283168\mathrm{m}^3}{1\,\mathrm{ft}^3} \bullet \frac{1.225kg}{m^3} \bullet \frac{1000\,\mathrm{grams}}{1\,\mathrm{kilogram}} = [x] \bullet 0.0096356\frac{g}{s}$$

The input voltages corresponding to the temperatures of the fluids at their perspective stages are conditioned and used to determine the heat flows in the system. The system calculates the heat into the system, the heat transferred through the thermoelectric modules, and heat lost in other system components.

The orange box contains the five temperature conditioning systems as shown in Figure 21. Input 1 is the voltage signal generated by the thermocouple, conditioned by the AD594 chip, and sent to the data acquisition board. It is then passed through a low pass filter. This removes the noise present in the input signal. The gain of 10 is the standard gain for inputs into dSPACE. After this amplification, the signal is then converted to degrees Celsius. This conversion is realized by a lookup table that correlates temperature to experimentally determined AD594 voltage output. Only the thermocouples on the liquid side were calibrated. For the two air inputs, a lookup table provided by Analog Devices was employed because the thermocouple calibrator would not reach the temperatures being measured.

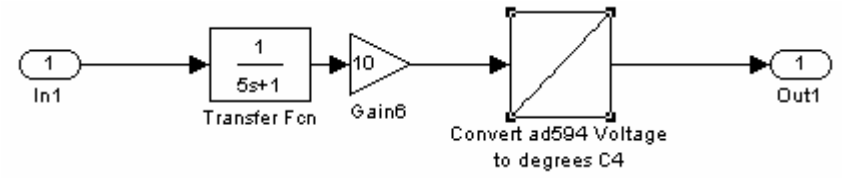

Figure 21 AD594 voltage to temperature

The pink boxes convert the temperature differences into heat transfer rates for both flows using the user inputted flow rates. Shown in Figure 23 is the conditioner for the liquid loop. This subsystem multiplies the fluid temperature difference (input 2) by conversion

factors and the user inputted flow rate to determine the heat quantity in watts using the equation: $q = \dot{m} \cdot cp \cdot \Delta T$. A lookup table is included because the specific heat of the antifreeze mixture varies with temperature. Inputs 1 and 3 are the temperatures of the flow. These are averaged to find a suitable specific heat value. As the flowmeter measures in gallons per minute, the following conversions are required where x is the user inputted volumetric flow rate in gallons per minute. Heat flow is found using:

$$Q = [x]\frac{gallons}{minute} \bullet \frac{1minute}{60\,\mathrm{sec}\,onds} \bullet \frac{0.003785m^3}{1gallon} \bullet \frac{1056kg}{m^3} \bullet \frac{4186.8\frac{J}{kg \cdot K}}{1\frac{Btu}{lb \cdot °F}} \bullet [c_p(\frac{Btu}{lb \cdot °F})] \bullet [\Delta T(°C)]$$

$Q = [x] \bullet 278.94 \bullet [c_p] \bullet [\Delta T]$. Figure 22 is a depiction of the lookup table used in the model relating the specific heat of the liquid mixture to temperature.

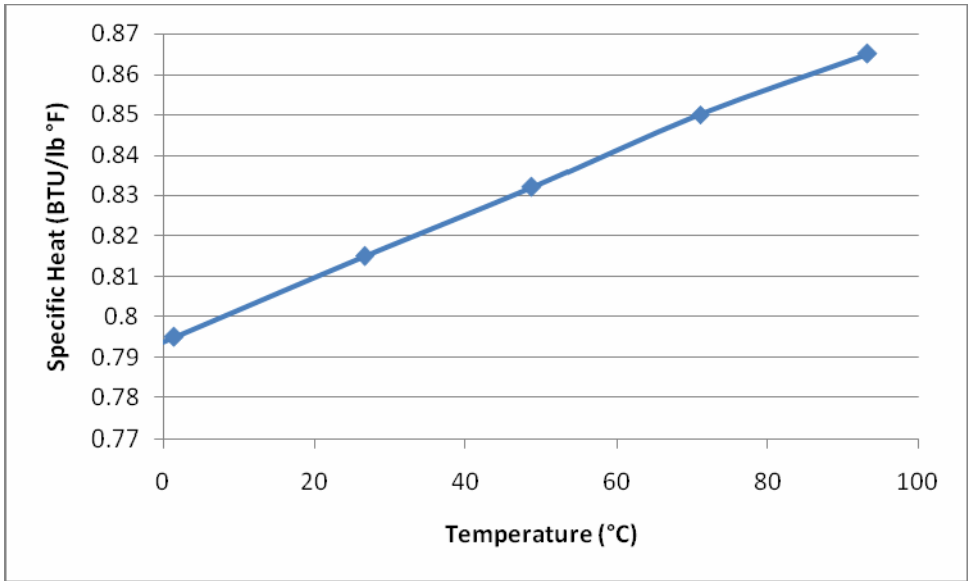

Figure 22 Specific heat of liquid solution as function of temperature

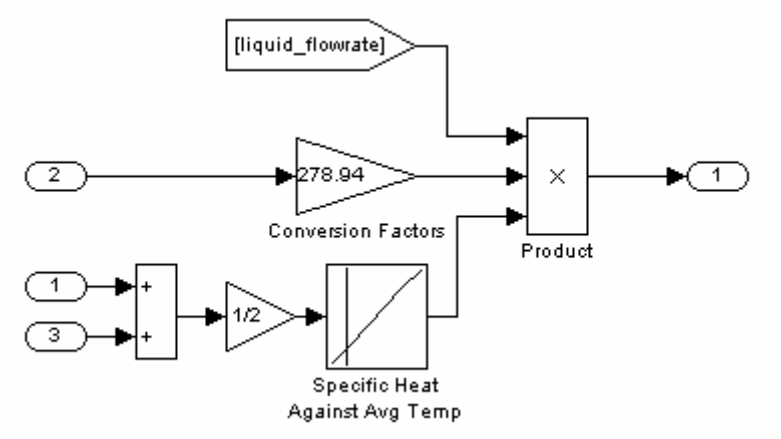

Figure 23 Convert liquid temperature difference to heat

The air heat subsystem in Figure 24 follows closely with the methodology used for calculating the heat transfer in the liquid loops.

$$Q = [x]\frac{\text{ft}^3}{\text{hour}} \bullet \frac{1\,\text{hour}}{3600\,\text{seconds}} \bullet \frac{.0283168\text{m}^3}{1\,\text{ft}^3} \bullet \frac{1.225kg}{m^3} \bullet [c_p \frac{\text{J}}{\text{g} \cdot \text{K}}] \bullet \frac{1000\,\text{grams}}{1\,\text{kilogram}} \bullet [\Delta T]$$ [x] is the user inputted volumetric flow rate, x, is in standard cubic feet per hour. This reduces to: $Q = [x] \bullet 0.009693 \bullet [c_p] \bullet [\Delta T]$

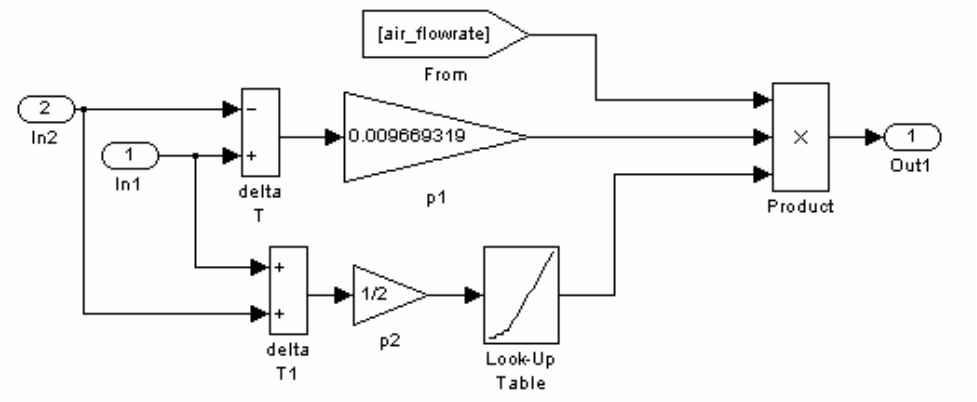

Figure 24 Air heat transfer calculator

Figure 25 is the subsystem that calculates the power generated by the thermoelectric modules. It uses the relation:

$$P = \frac{V^2}{R_{Load}}$$

Where V is the voltage developed by the modules and R_{load} is the value of the load resistance.

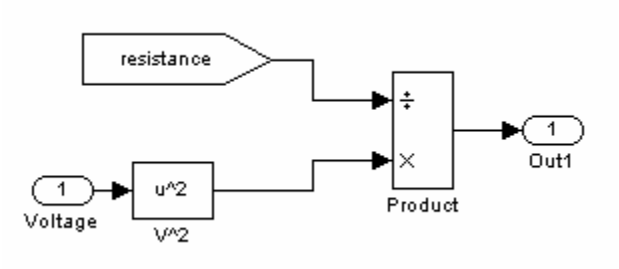

Figure 25 Subsystem that calculates power generated by modules

Components Specific to Radiator Test

Shown in Figure 26 is the control system for maintaining the desired liquid temperature. It sets the on time of the electric heater by utilizing a pulse width modulated signal. The setup outputs a 4 Volt signal in order to switch the solid-state relay on and a 0 Volt signal to turn the relay off. The pulse width modulation was achieved using a triangle wave and the error present in the temperature difference between actual and desired liquid temperature. A 2 Hz wave was used as to not exceed the switching capability of the dSPACE's analog output signal. Additionally, the heater has a high time constant, so this would not affect the operation. The error was normalized to range from 0-1 during steady state operation. If the error is greater than the triangle wave, the relationship operator outputs a 1, which is amplified into a 4 Volt signal. If it is less, the system outputs a 0. This control of the heater will allow the calculation of input heat into the system. After measuring the voltage and current that the heater is requesting, its actual power output will be calculated. By calculating the percentage on time of the heater and multiplying

this by the generated power, it is possible to determine the average power delivered over a discrete time period.

Referring to the PID controller, it was found that the integral term caused an undesirably high overshoot. Attempts to minimize this overshoot by incorporating a larger derivative term failed because of the noise present in the temperature voltage signal. During steady state operation, the derivate would amplify the noise, leading to a loss in stability. Additionally, the derivative term will cause the system to take longer to reach steady state, and as the system takes upwards of 10 minutes to heat up, this was undesirable. Therefore, a solution that minimized the overshoot from the integral was sought.

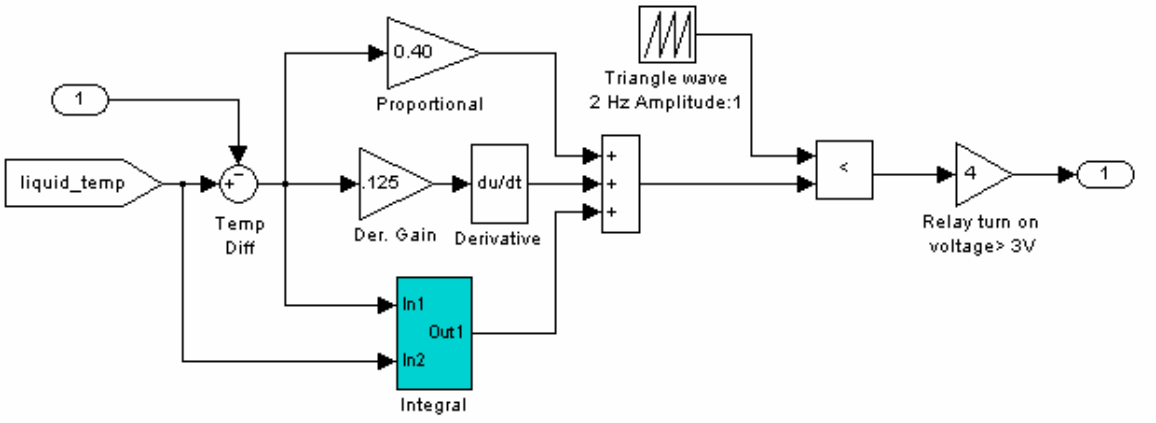

Figure 26 PID and PWM control for liquid heater

In order to minimize this overshoot error, the integral term was configured to not 'turn on' and integrate the error until the actual temperature was within 10% of the desired value. Please see Figure 27 for the Simulink diagram. This led to an overshoot of only 4 degrees in a 60-degree jump. The steady state error was reduced an amount under the error present in the thermocouples and their conditioners by the integral term. The usage of this controller for the water temperature during radiator testing allows for the OMEGA

PI controller to be used to regulate air inlet temperature, thus creating opportunities to investigate the performance of the thermoelectric modules based on air inlet temperature.

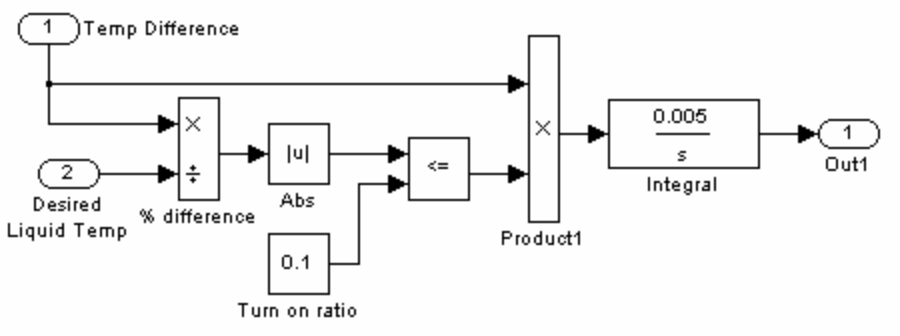

Figure 27 Integral portion of PID control (green box in Figure 26)

Components Specific to Exhaust Test

For the exhaust test, the external controller regulated the inlet air temperature and the heat flux into the system. The liquid loop heater was not engaged at any time. To control the temperature of the liquid loop and to remove the added heat, the fans were engaged. The fans were controlled using a Simulink PI controller and a hardware based PWM controller. The PWM chip was regulated by the relationship (% On Time) = -27.25 Voltage(input) + 124. It is 100% on at zero volts and 0% on at 3.6 volts. The saturation control is used to prevent the board from outputting an unnecessarily high voltage.

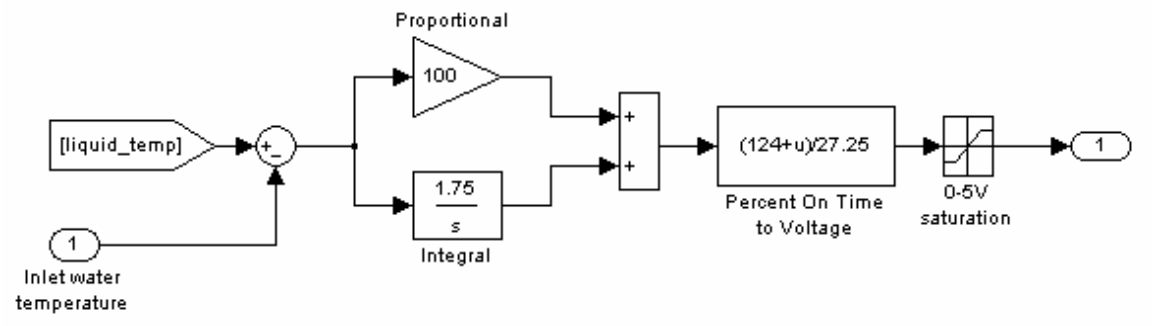

Figure 28 Fan controller

The inlet temperature to the air side heat exchanger is used to determine the heat input to the system. The temperature difference across the exchanger is used to determine the heat passed through and the difference between the outlet and ambient temperatures is used to determine the heat not captured by the thermoelectric heat exchanger. The temperature rise of the liquid side across the heat exchanger is also noted and converted to a heat input.

Efficiencies

Realized thermoelectric efficiency is defined as:

$$\eta_{TE} = \frac{P_{gen}}{Q_h},$$

where P_{gen} is the power generated by the thermoelectric modules and Q_h is defined as:

$$Q_h = \frac{Q_{air} + Q_{liquid}}{2}$$

Q_{air} is calculated using the temperature drop across the air side of the heat exchanger and Q_{liquid} is found using the temperature drop across the liquid side. This averaging is done to minimize the errors that exist in the heat losses in the system. While this method ignores the generated thermoelectric power, other losses in the system are greater than the generated power, thus rendering this effect small. Total efficiency is defined as:

$$\eta_{total} = \frac{P_{gen}}{Q_{in}}$$

where Q_{in} is the heat input to the system. The previously developed equation:

$$\eta_{TE} = \frac{T_h - T_c}{\frac{4}{Z} - \frac{T_h - T_c}{2} + 2T_h}$$

is used to calculate the theoretical efficiency. This equation requires the knowledge of the ΔT across the modules and the temperature on one side. The cold side temperature of the modules is determined by adding 5°C to the fluid temperature to account for thermal resistances. The material properties of the thermoelectrics are referenced off of Table 1 at an average temperature. The open circuit voltage for the Peltier modules is measured and divided by the number of modules in series to give an average open circuit voltage across the ten modules. This is then converted to a ΔT.

Electrical Configurations

One question to be answered by the experiment was whether the electrical configuration of the modules would affect the net output of the modules. As the temperature of the fluids would change across the heat exchanger, the modules would have different operating temperatures, open circuit voltages, internal resistances, and ultimately, different power outputs. Therefore, four electrical configurations were tested. They are *all parallel, all series, 2 parallel by 5 series* and *5 series by 2 parallel*. The *2 parallel by 5 series* and *5 series by 2 parallel* can be seen in Figure 29 and Figure 30, respectively. *All serie*s means that each module's positive lead was connected to the subsequent module negative lead. *All parallel* means that the positive leads for all the modules were connected to the same potential and the negative leads to a separate potential.

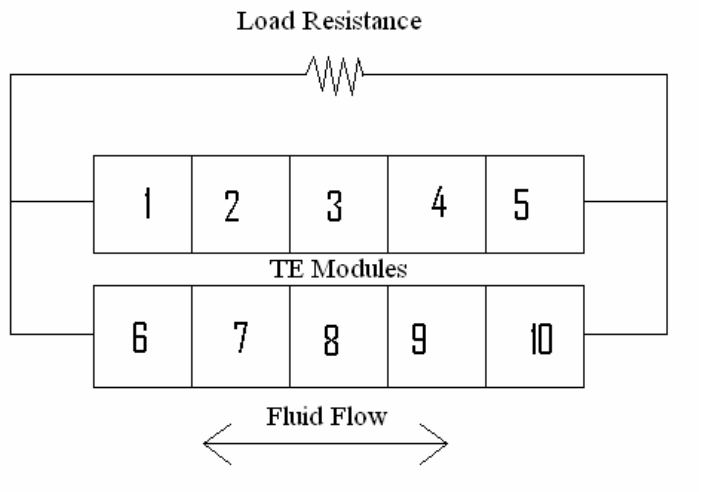

Figure 29 Electrical configuration for TE modules – 2 parallel 5 series

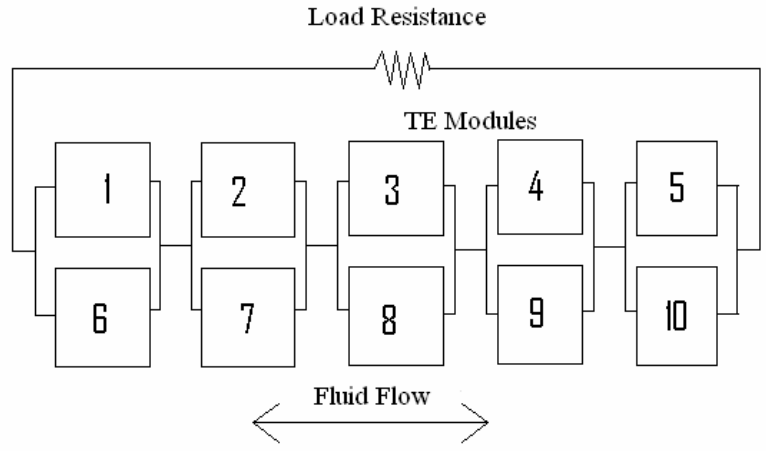

Figure 30 Electrical configuration for TE modules - 5 series 2 parallel

Discussion of Results

Exhaust Based Testing

From the initial stage of testing, it is seen that the maximum working temperature of the thermoelectric modules of 225°C is not reached. The maximum hot side temperature measured by the thermocouple placed in the heat exchanger is roughly 170°C. This temperature was validated as correct by using the open circuit voltage measured from the first thermoelectric module. After converting V_{OC} to temperature, it was added to the

cold side working fluid's temperature to determine the approximate range of the hot side temperature of the modules.

Output Power vs. Load Resistance

Included in the first round of testing was the determination of the relationship between electrical load resistance and electrical power produced by the thermoelectric modules. Theory states that for maximum power generation the load resistance must be varied to match the net internal impedance of the modules. The thermoelectric modules were connected in four different configurations: *2 parallel by 5 series, 5 parallel by 2 series, all series,* and *all parallel*, as discussed previously. The voltage across the thermoelectric modules was measured at various resistances and the electrical power was calculated. This experiment will help to answer the question of whether the output power will be affected by how the modules are electrically connected. All experimental parameters such as temperatures and flow rates were kept constant for this experiment. The initial rise in power as resistance increases from zero is a parabola, but the drop as resistance increases towards infinity is not. As can be seen, it is a gently sloping line. This follows the 1/x law.

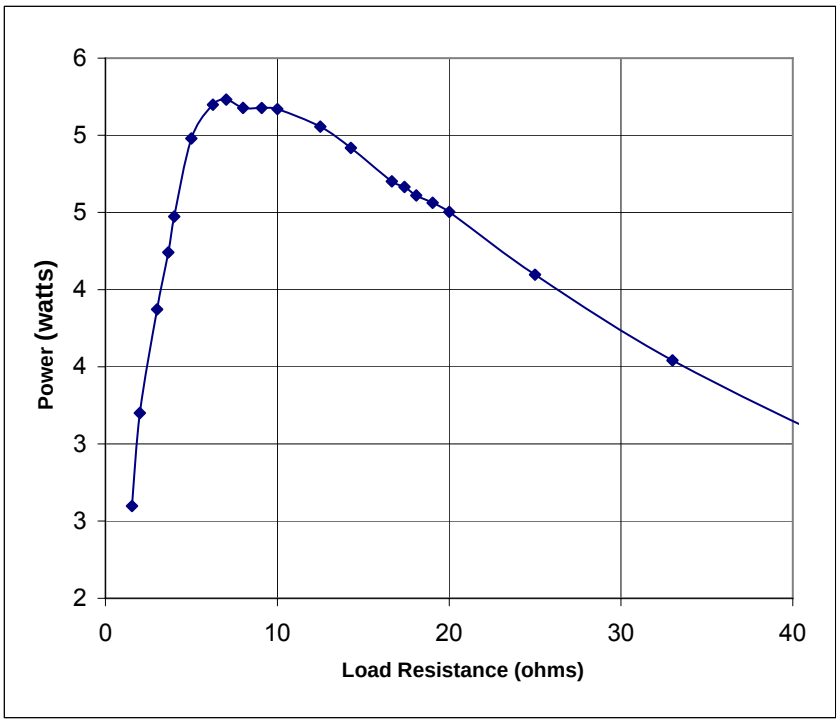

Figure 31 Output power vs. load resistance – 2 parallel by 5 series

As referenced from Figure 31, the maximum power is reached at 7 ohms and is 5.23 watts. By plotting the voltage against current, the VI plot can be obtained. The slope of this plot is –8.9 ohms. According to theory, the maximum power would be reached with:

$$R_{Load} = \frac{V_{OC}}{I_{ISC}}$$

Please reference Figure 32 for a plot of the VI curve. The open circuit voltage is 13.7 Volts and the short circuit current is 1.53 amps. The electrical load resistance would be set equal to the slope of the plot. However, with a load resistance of 9 ohms, only 4.6 Watts of power was generated. Therefore, the resistance calculated from the VI curve yields a value that will lead to lower power generation.

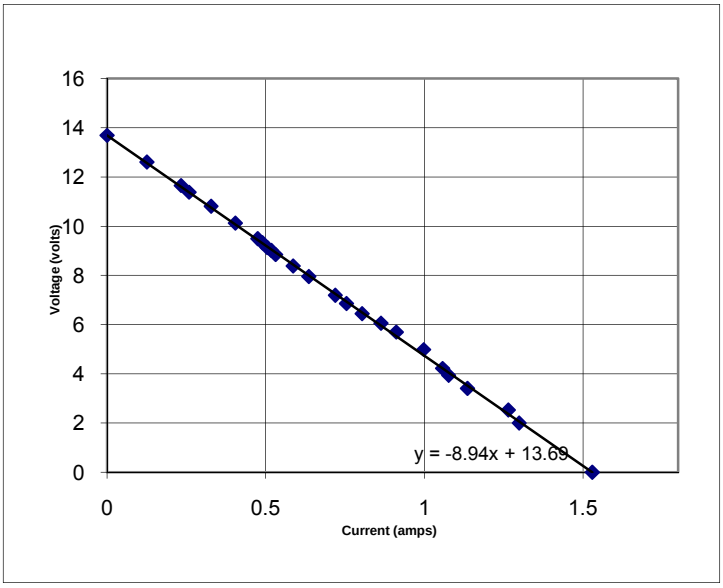

Figure 32 VI curve for 2 parallel by 5 series

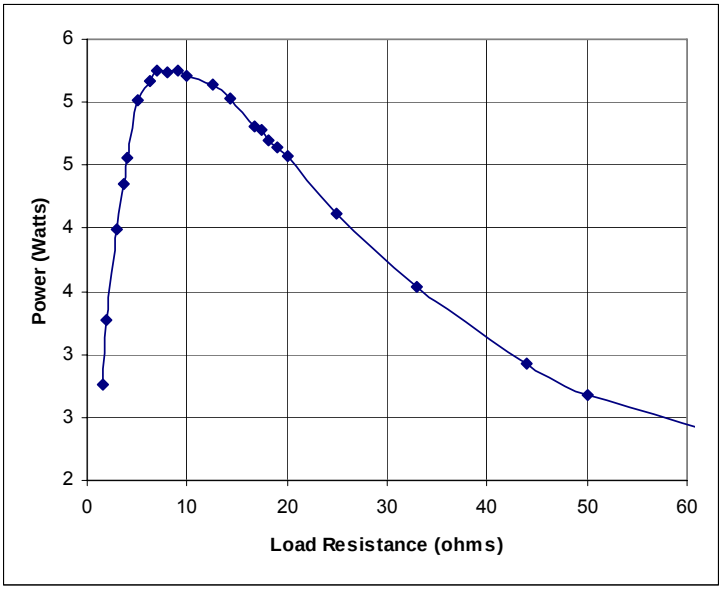

Figure 33 Output power vs. load resistance - 5 series by 2 parallel

With a different configuration of two sets of five modules in series wired in parallel, the maximum power generated was 5.25 Watts at 9.09 Ohms. Please reference Figure 33 for a plot of power vs. load resistance. Again, from the VI plot, the slope was –8.7 ohms. This falls closer to the experimentally determined maximum power resistance. However, with this configuration there is no gain of power over the previous setup.

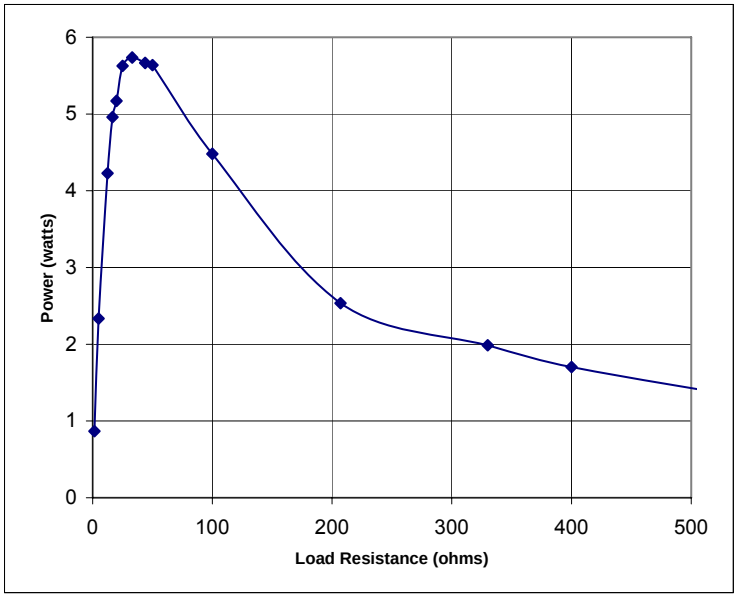

Figure 34 Output power vs. load resistance - all series

The curve in Figure 34 was created with all the modules electrically connected in series. As can be seen, the net resistance for the setup is higher. The maximum power was found to be 5.66 watts at a load resistance of 44 ohms. The slope of the VI line was found to be –35.7 ohms. Again, the two resistances did not match up. However, it is seen that there exists a wide range of resistances where power generated is within 2% of the maximum generated power. This configuration shows an increase in power over the two previous configurations.

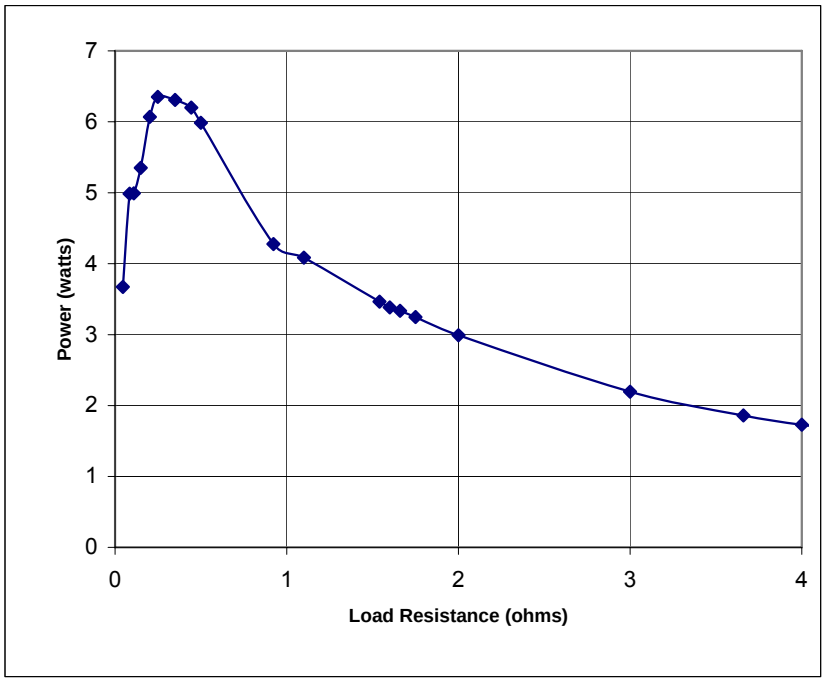

Figure 35 Output power vs. load resistance – all parallel

The curve in Figure 35 was found with all of the modules connected in parallel. This resulted in very small net impedance for the setup. The power output peaked at 6.35 watts at a load resistance of 0.25 ohms. Surprisingly, this configuration yielded the highest power output out of the four. The slope of the VI curve was calculated to be -0.29 ohms. At such low resistances, contact resistance plays a major factor. However, this resistance is unknown and varies between each load resistance. Additional 0.5 and 0.1 ohm resistors were placed in parallel with the original 10 resistors in order to drop the load resistance low enough. From these experiments, it was found that the resistance given by the VI curve could only be used as a guideline for finding the actual load resistance. Table 2 contains the data discussed previously.

Table 2 Peak power for different module configurations

Configuration	Load Resistance (ohms)	Max Power (watts)	Total Current (amps)	Current Through Each Module (amps)
2 Parallel by 5 Series	7.02	5.23	0.863	0.4315
5 Series by 2 Parallel	9.09	5.25	0.76	0.38
All Series	44	5.66	0.3586	0.3586
All Parallel	0.25	6.35	5.04	0.504

By normalizing the resistances on the previous power vs. load resistance graph, one can plot the curves on the same plot. This is shown in Figure 36. As can be seen, the curves all follow roughly the same shape. Figure 37 contains the theoretical power output

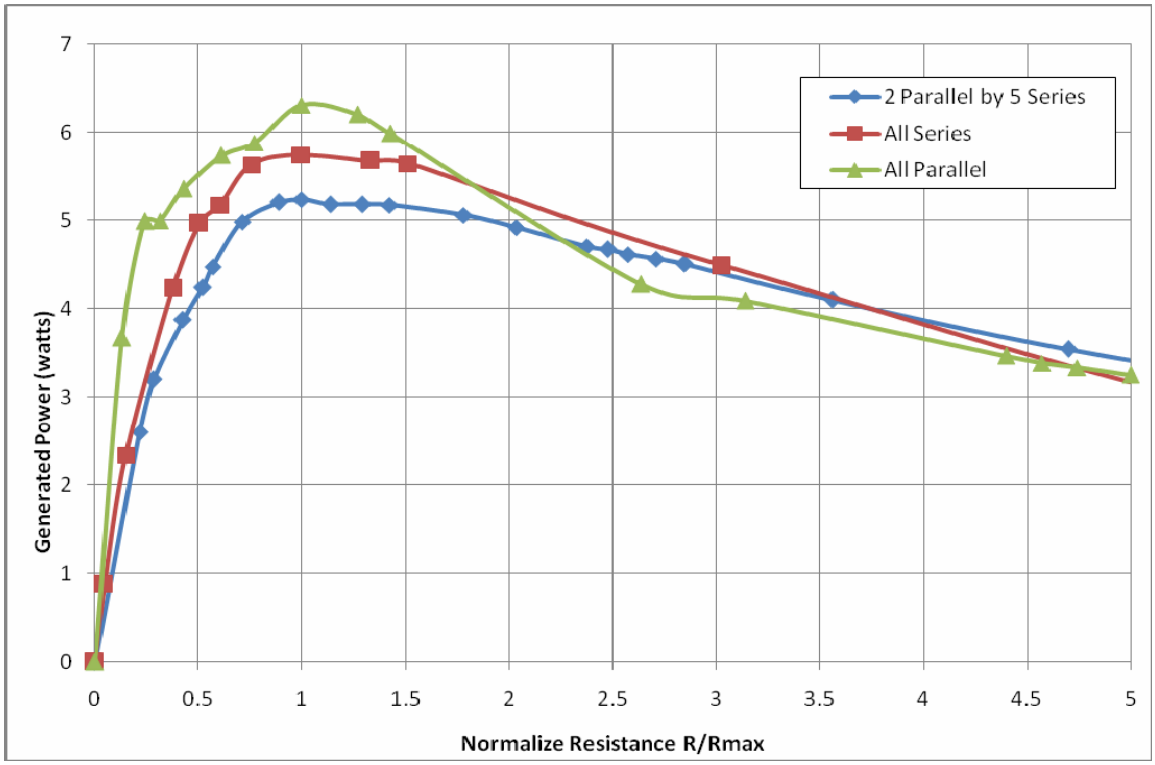

Figure 36 Generated power vs. normalized resistance

plotted against the normalized resistance for the three cases shown in Figure 36. For the *all parallel* and *2 parallel by 5 series* cases, the curves follow closely together. However, for the series case, they diverge. The exact reason for this 1 watt difference is unknown.

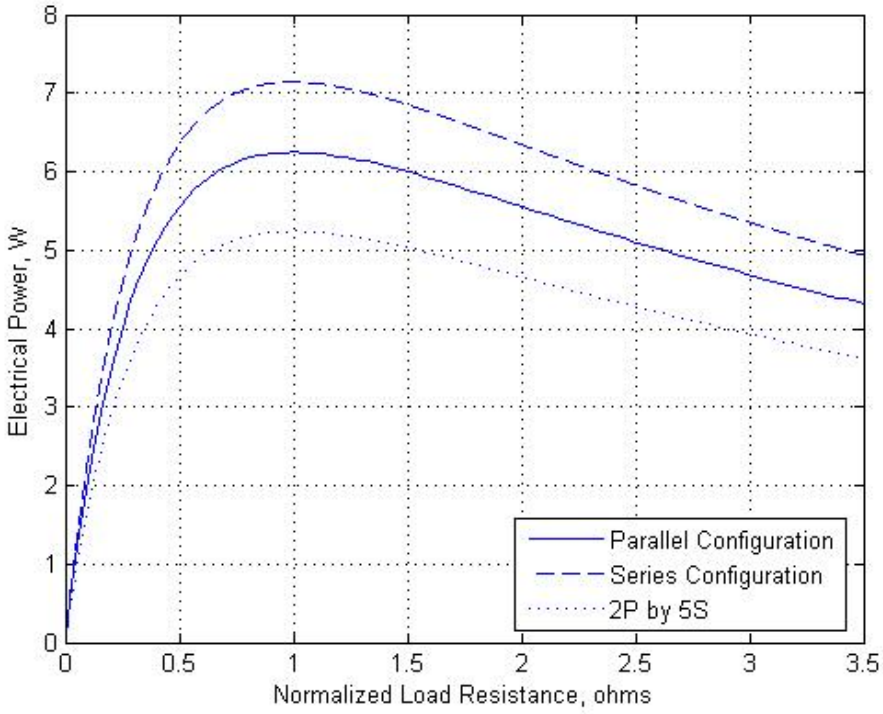

Figure 37 Theoretical electrical power output vs. normalized load resistance

Power and Efficiency in Relation to Q_{hot}

Next, generated power and thermoelectric efficiency were found in relation to the heat passing through the thermoelectric modules. These were determined with the losses in the system unaccounted for. Therefore, the efficiency of the modules is lower than what actually exists in the system. These two plots were generated at constant liquid coolant temperature and constant fluid flowrates. The modules were connected *2 parallel by 5 series*. The inlet air temperature was adjusted, thus causing a change in the heat transfer. As seen in Figure 38, efficiency raises as the heat that passes through increases. This follows the Carnot efficiency trend for a generator. From Figure 39, generated power increases as the heat transfer grows larger.

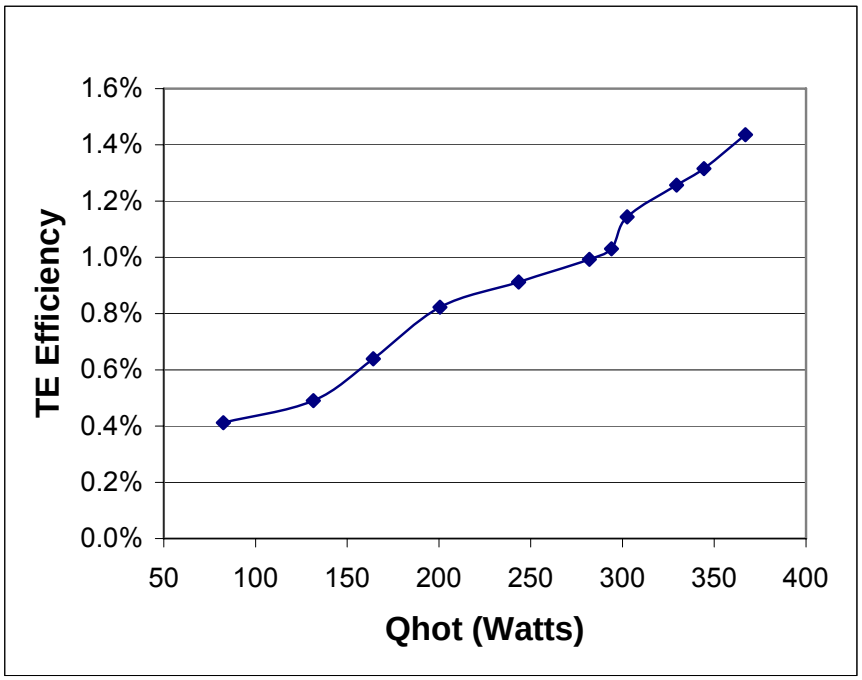

Figure 38 Thermoelectric efficiency as a function of Qhot

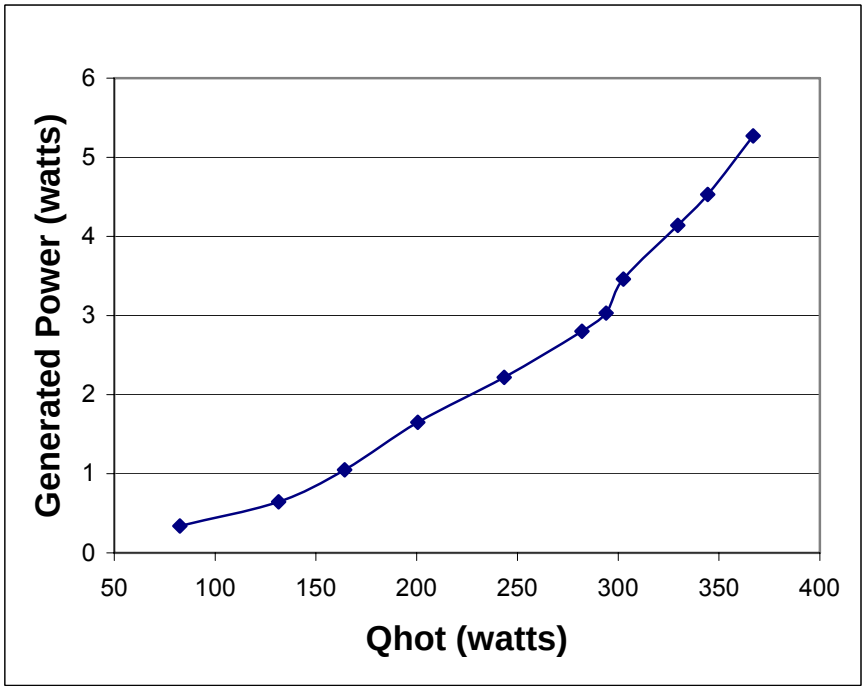

Figure 39 Thermoelectric power as a function of Qhot

After several tests, the average inlet and outlet air temperatures were noted, along with the temperature differences across the thermoelectrics. From these numbers, the original

script, which was utilized to calculate the dimensions of the heat exchanger, was modified to incorporate this new experimentally determined data. As can be seen in Figure 40, the air temperature drops drastically across the heat exchanger and is very close to the actual temperature of the base after traveling only halfway through. This plot was obtained for a liquid coolant temperature of 90°C. Metal base temperature was calculated by adding several degrees to account for thermal resistances and the ΔT to the coolant temperature. From this plot, it was decided that the addition of another electrical air heater in the air loop was necessary. It would allow for a higher flow rate of air at the same temperatures. The convective heat transfer coefficient was calculated to be 36 W/m^2K.

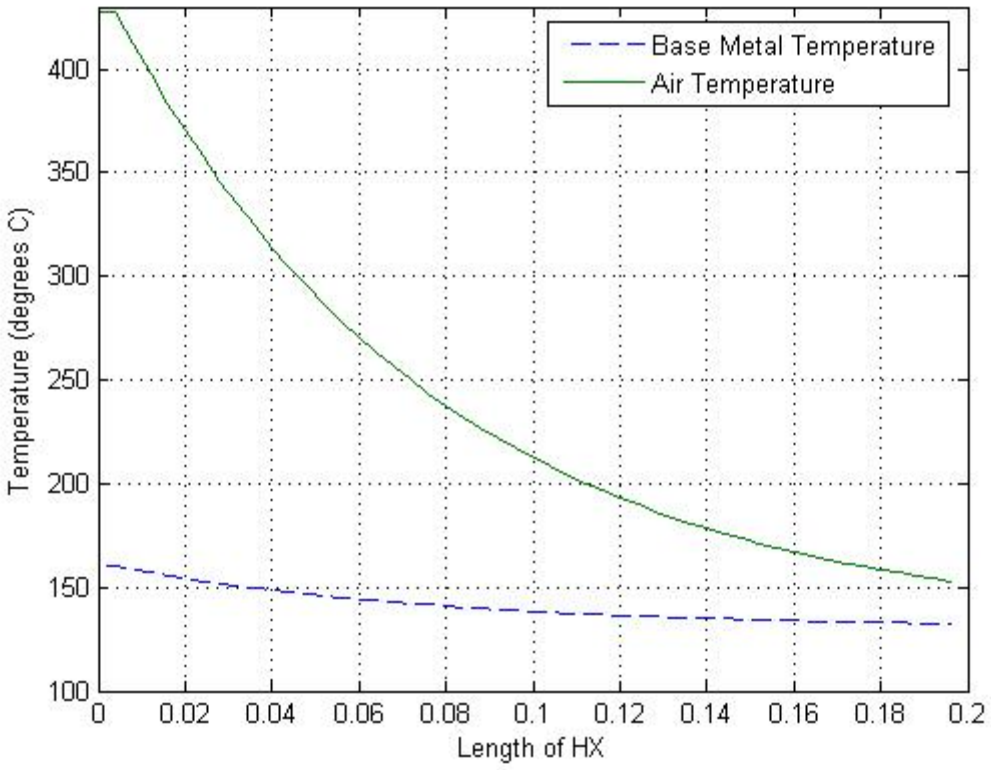

Figure 40 Theoretical temperature distribution across airside heat exchanger

Power vs. Load Resistance with Additional Air Heater

After the installation of the additional air unit, maximum power vs. load resistance plots were experimentally determined. This time, *all parallel*, *all series*, *and 2 parallel by 5* series were tested. *5 series by 2 parallel* was not tested because experimental data showed that its maximum power output was very close to *2 parallel by 5 series*. As was expected the power output increased dramatically up to over 10 watts. All of these power vs. load resistance curves were found with the same conditions. Air inlet temperature was 440°C. The temperature of the liquid coolant rose from 55°C to 62°C across the heat exchanger.

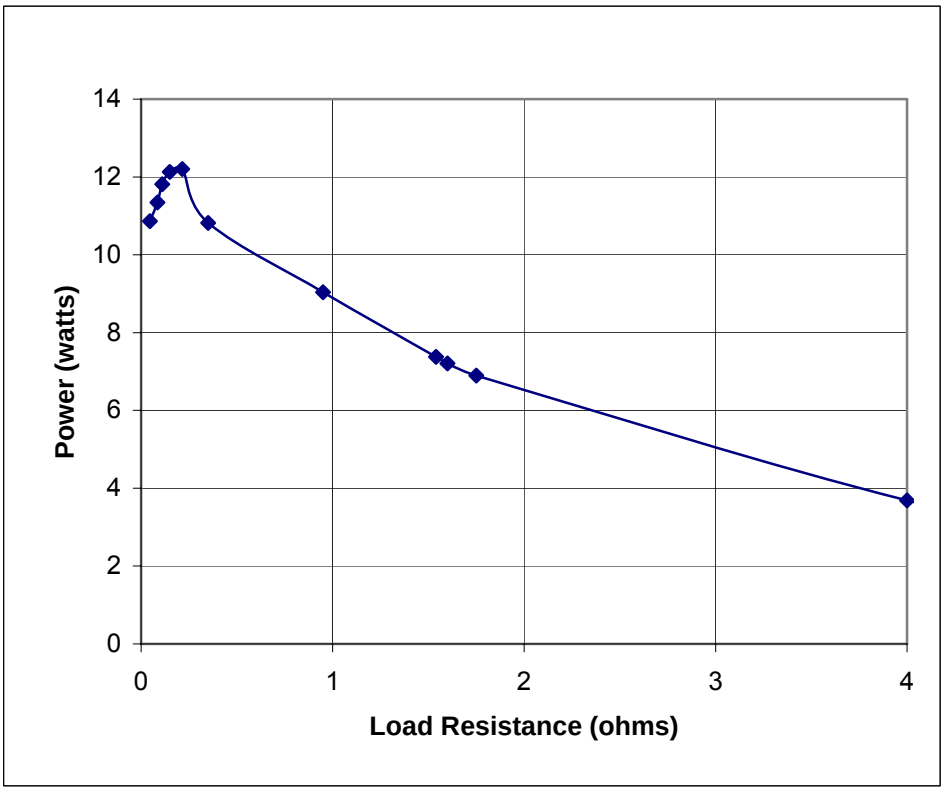

Figure 41 Output power vs. load resistance – all parallel 2 heaters

In Figure 41, the maximum power reached is 12.2 Watts at a load resistance of 0.215 ohms. This plot was generated using *all parallel*. There is uncertainty in these measurements due to contact resistances.

Figure 42 and Figure 43 show the output power plotted against load resistance for *2 parallel by 5* series and *all series*, respectively. *2 parallel by 5 series* reaches a maximum power of 11 watts at a load resistance of 9.09 ohms. *All series* has a maximum power generation of 11.5 watts at 44 ohms. From these three plots, it was decided to pursue further testing with the modules placed electrically in series. This course was chosen because it had a higher power output than the 2 parallel by 5 series combination. In regard to the *all parallel* configuration, it produced slightly less power. However, the uncertainties present in the *all parallel* configuration led to the decision to choose the series configuration.

Figure 42 Output power vs. load resistance – 2 parallel by 5 series 2 heaters

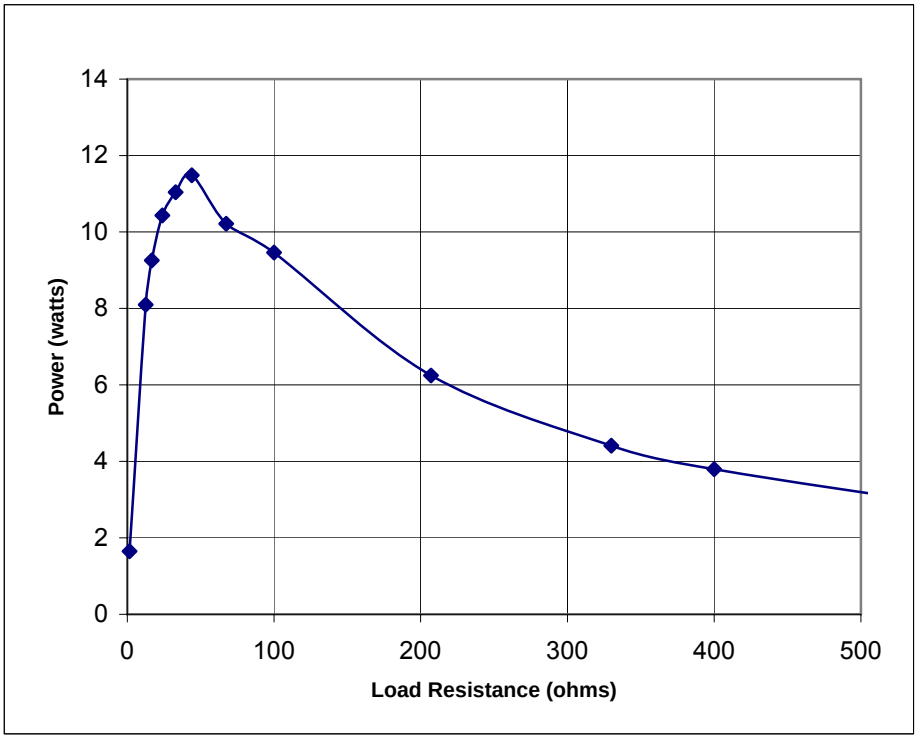

Figure 43 Output power vs. load resistance – all series 2 heaters

Again, the previously discussed Matlab script was modified to include the additional heat input from the second air heater. Using the same methodology to determine base temperatures, Figure 44 was generated. As can be seen, the temperature of the hot air does not drop so close to the base metal temperature. This allows for a higher heat transfer and power generation as:

$$P_{\max} = \frac{V_{OC}^2}{4R_L}$$

where V_{OC} is directly related to the temperature difference across the modules. However, the heat exchanger is not as efficient because a higher temperature stream of air is exiting. With one air heater, the heat exchanger was realized efficiencies as high as %, and now it is a maximum of %. While this would appear to lower overall efficiency

$$\eta = \frac{P_{gen}}{Q_{in}}$$

in actuality the percentage increase in P_{gen} is greater than the percentage increase in Q_{in}.

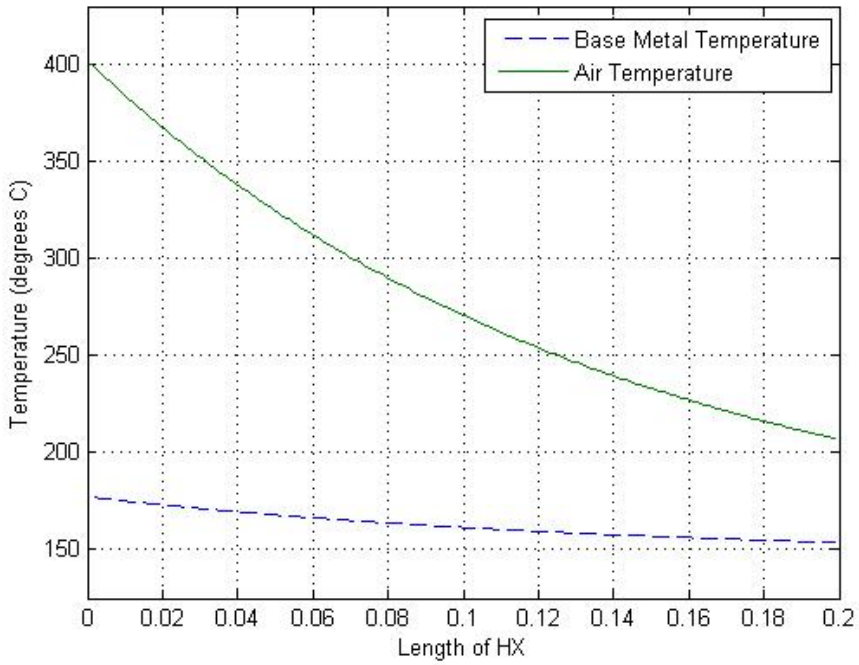

Figure 44 Theoretical temperature across airside heat exchanger – 2 heaters

Generated Power and Efficiency with Additional Air Heater

Additional tests were run after the installation of the additional air heater. As can be seen in Figure 45, the generated power reaches up to over 11 watts with a Q_h of 550 watts. Referencing Figure 46, it is apparent that the efficiency of the modules increases along with Carnot efficiency. Figure 47 shows the relation between generated power and Q_{in} and Figure 48 contains the relation between overall system efficiency against $Q_{in,}$ where Q_{in} is defined as the heat input into the system. Figure 49 shows the scattering of data of the measured heat flows in the water and air side. The circles are Q_{air} and the squares are Q_{water}. Averaging these values at each trial yields Q_{avg} as depicted with the triangle data points. The maximum reached efficiency of the overall heat exchanger was 1.2% with a

thermoelectric efficiency of roughly 2%. A scaling by a factor of 30 to realize what would actually be in a car yields 30x11 watts = 330 watts recovered electrical power.

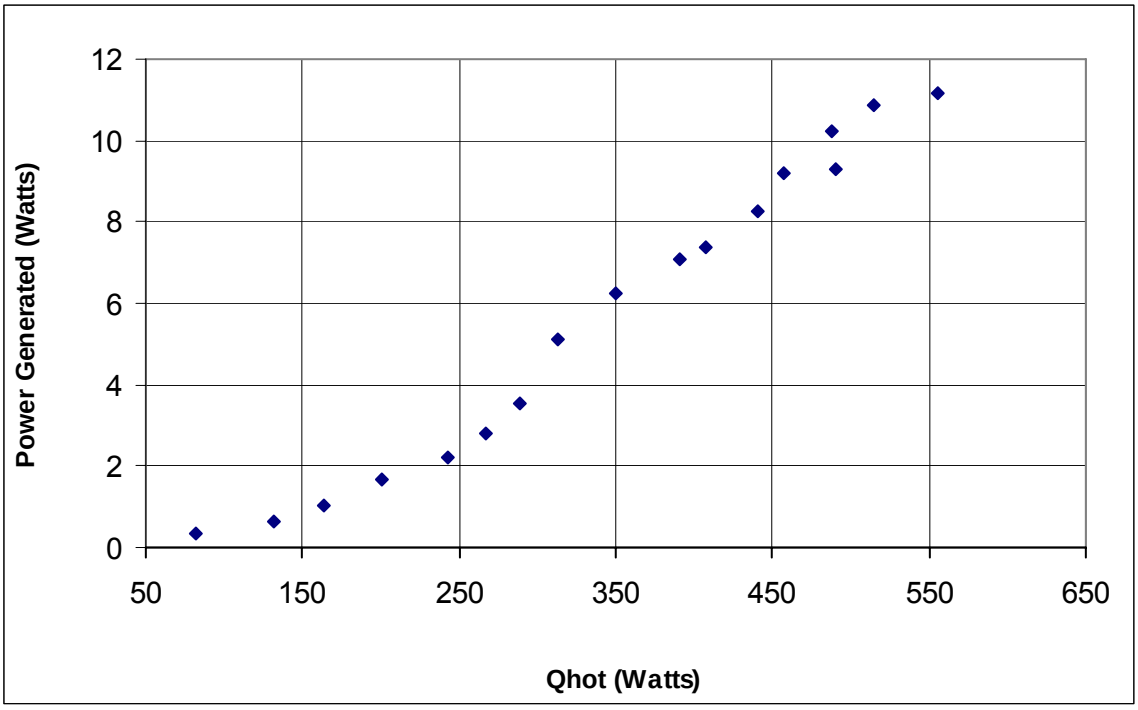

Figure 45 Generated Power vs. Qhot

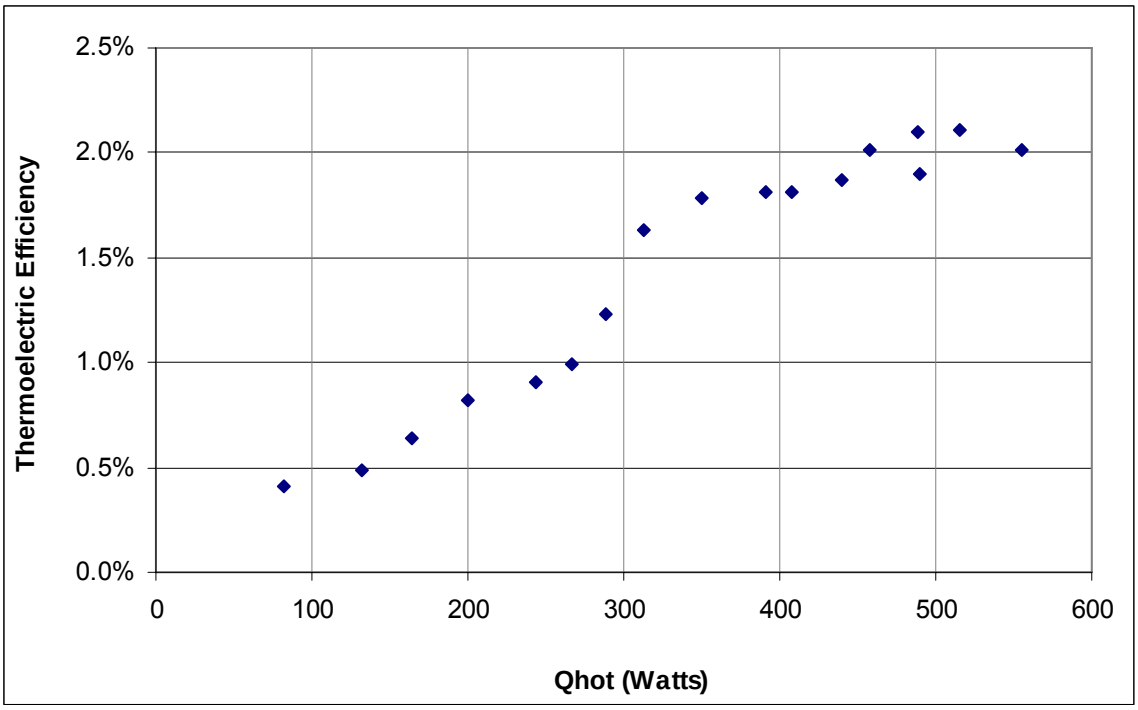

Figure 46 TE efficiency vs. Qhot

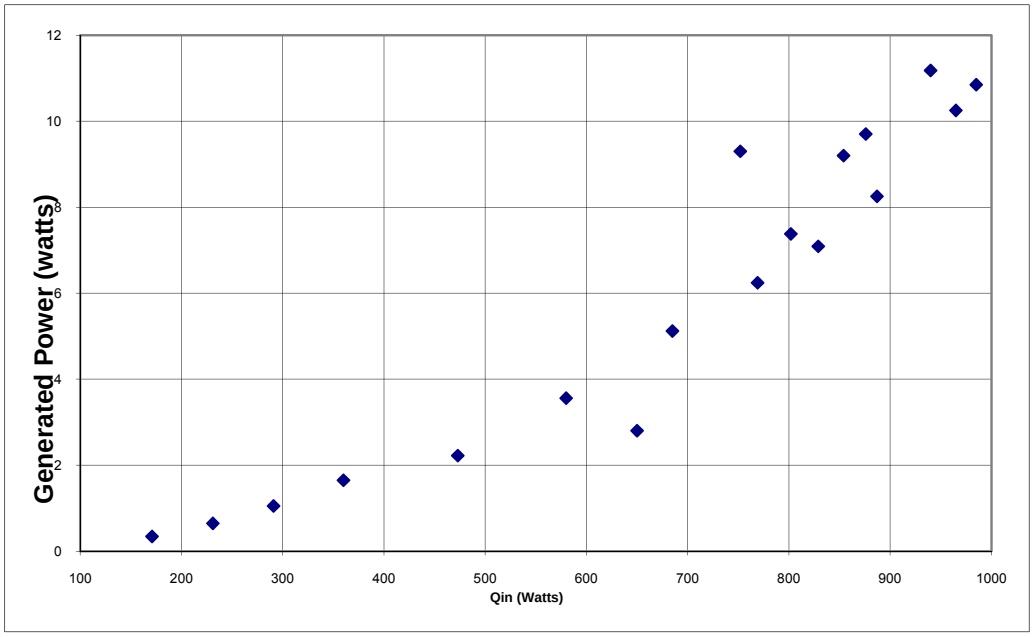

Figure 47 Power generated against heat input

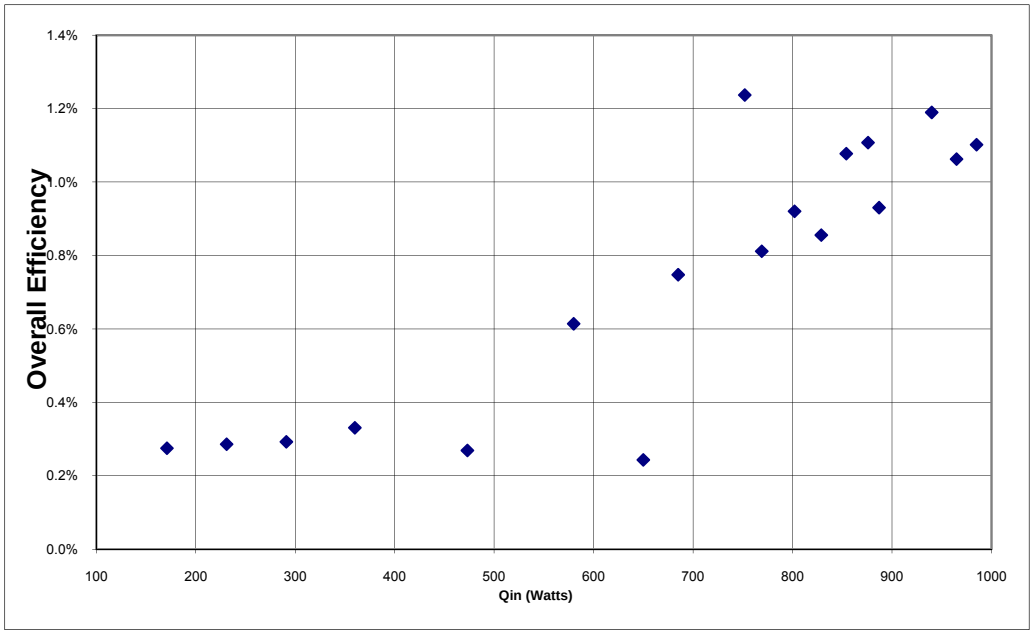

Figure 48 Overall efficiency against heat input

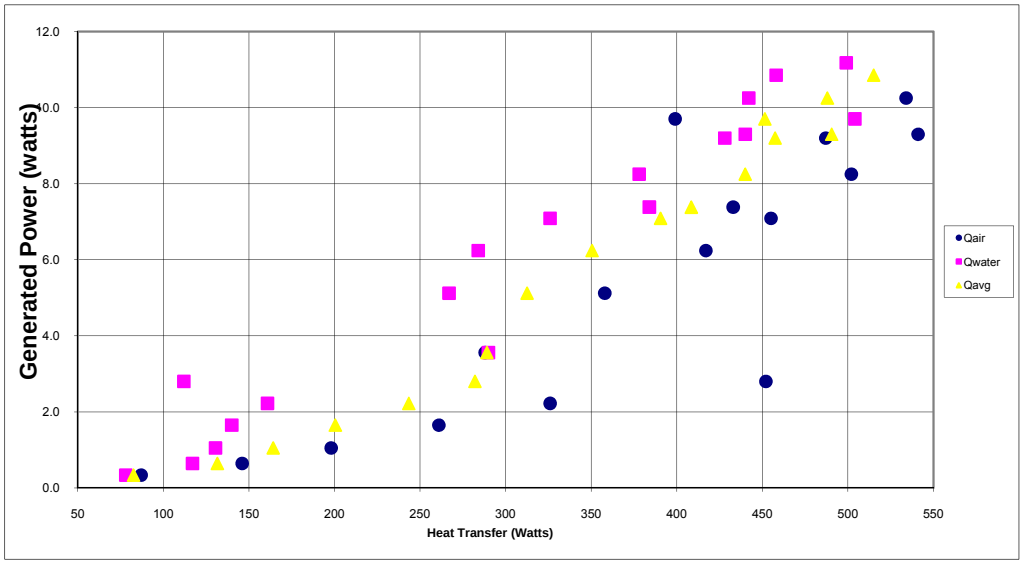

Figure 49 Heat flows against generated power

As referenced from Figure 49, the measured air heat flow is generally greater than the measured water heat flow.

Radiator Based Testing

Due to the lower temperatures present in the radiator of 100°C as compared to 400-500°C in the exhaust system, the radiator in this experimental setup will not generated as much power as the exhaust system. During the first stage of testing, plots such as that in Figure 34 of power vs. load resistance were generated. They look just like the ones viewed in earlier sections, just with lower output power, and will not be shown here.

The maximum power generated using the *all series* configuration was 1.07 watts with a 100°C hot liquid temperature cooled by compressed air at ambient temperatures. *All series* was the only electrical configuration tested for the radiator. Open circuit voltages were ~1.2 Volts per module, which is far less than the exhaust testing, which reached 4 Volts per module. A low V_{oc} correlates to low power with the equation

$$P_{\max} = \frac{V_{oc}^2}{4R_{load}}$$

Conclusions and Recommendations

Several design mistakes were made during the design and instrumentation of this experiment that will need to be corrected in order to more accurately characterize the thermoelectric modules performance.

Temperature measurement and control issues on the liquid loop plague the experiment from the beginning. After the removal of electrical noise through adding a capacitor between the +12V and ground, the AD594 chips still had error in their output. One reason for this was thermal drift. As the experiment ran, the chips would heat and cool depending on air currents and the heat expelled by the system. During this experiment, it was not plausible to move the signal conditioning chips, so a vapor barrier was implemented. A piece of cardboard was placed between the chips and the heat exchanger, which is the largest heat source. The thermocouples also had to be calibrated using a temperature calibrator. A wire was run connecting the thermocouple probes with ground. If time constraints didn't exist, the chips would have been relocated to an area that had a higher degree of thermal isolation. Additionally, the fluid flow rate was reduced in order to increase the difference between the inlet and outlet liquid temperatures.

The initial design of the thermoelectric heat exchanger included ten bare fine gage butt-welded thermocouple wires (0.005" diameter). These thermocouples were placed at the front of each thermoelectric module, perpendicular to the fluid flows. These were intended to give the surface temperature of the modules along the heat exchanger. However, the thermocouples all experienced a ground loop with the aluminum heat exchanger and did not provide a useful output. The thermally conductive grease, while

electrically insulating, did not provide enough insulation for the thermocouples. As this was discovered after the heat exchanger was assembled, it was hoped that the experiment could be fully characterized without these temperatures. One 1/8" diameter thermocouple was installed as a safety measure to ensure that the temperature of the heat exchanger did not exceed the maximum working temperature of the modules. It was soon found out that more temperature measurements were needed in order to determine where all of the heat losses occurred and their relative sizes. Therefore, it would be useful to attempt another method of surface temperature measurement of the modules, or to drill into the heat exchangers and place small diameter thermocouples, less than 1/16-inch diameter, into various points in the heat exchanger.

Another design flaw introduced itself in the bolts that were utilized to secure the two sides of the heat exchanger to each other. They provided a direct, not insulated path for heat transfer between the fluids. While in a normal heat exchanger this is not a problem, for a thermoelectric heat exchanger where the objective is to route all of the heat through the modules, it is. Additionally, it obscured the heat transfer calculations that the efficiencies of the modules and heat exchanger were based off of. Less heat was actually being transferred through the heat exchanger than was calculated. The calculation for the heat transfer through the bolts is difficult and extremely convoluted. If time allowed, the thermoelectrics would be removed from the heat exchanger and tests would be run to characterize just the heat exchanger without thermoelectrics.

When testing the different configurations, exhaust and radiator, different air flows are needed. This means that different air flow meters will need to be used. The exhaust based testing is utilizing ~250 SCFH air flow rate and 0.4 gpm water flow rate. The

radiator testing needs a much higher air flow rate than the current flow meter can offer of 400 SCFH. Upon performing an effectiveness analysis of the heat exchanger, it was found that the C_{air} and C_{liquid} differed by two orders of magnitude. While this did not affect the exhaust testing, the radiator testing was effected drastically. The air was not able to adequately remove the heat coming from the cold side.

Unfortunately, the intended radiator characterization was never completed. This would have tabulated duty cycle time for the fans with coolant temperature and heat dissipation. It would have allowed for the control of the heat removal to be a greater degree of accuracy. It would have also proved useful to the Simulink model.

During testing, it was found that the parallel configuration had the highest power output. Unfortunately, the peak powers occurred in ranges outside the range that the parallel resistances could reach. If time allowed, additional 10-watt resistors with low resistances would have been installed. Ideal resistances would be in the 0.1-1.0 ohm range. A potentiometer could be installed in order to allow creating resistances between the 1000 currently realizable resistances. Ideally, an electronically controlled load would be installed in replacement of the ceramic resistors.

Furthermore, it would be helpful if a tool was designed that would analyze the thermal, mechanical, and electrical configuration of the TE modules and heat exchanger and optimize the parameters for optimum configuration and ultimately the maximum generated power output. This tool would help the designer in selecting components for the system. Additionally, the tool would allow for the inputs to the system, i.e. flowrate and temperature of the fluid, to control the electrical load in order to impedance match the thermoelectric modules.

Scaling up the heat exchanger to realize the heat fluxes in an automobile does not lead to enough generated power to displace the alternator. However, with improved materials that have a higher ZT along with improved heat exchanger design, the potential does exist. The thermal mass of the exhaust massed heat exchanger would have to be small in order to respond rapidly after ignition and begin generating power. The radiator heat exchanger would be in a quasi-isothermal state where the coolant temperature will only vary by several degrees during driving after steady state is reached. The exhaust system's input fluid will vary with driving conditions.

References

1 **Heywood, J.B.** *Internal Combustion Engine Fundamentals*. (McGraw-Hill, New York, 1988).

2 **Angrist, S.W.** *Direct Energy Conversion*. (Allyn and Bacon, Boston, 1976).

3 **Subramaniam, V.V.** ME H610: Direct Energy Conversion Class Notes. (Ohio State University, Columbus, 2006).

4 **Venkatasubramanian, R. and , et. al.** Thin-film thermoelectric devices with high room-temperature figures of merit. *Nature*, 2001, **413**, 597-602.

5 **Bass, J.C., N. B. Elsner, and R. Slone**. Design Study and Experience with Thermoelectric Generators for Diesel Engines. *Automotive Technology Development Contractor's Meeting*Dearborn, MI, 1991).

6 **Bass, J.C., Elsner, N.B. and Levitt, F.A.** Performance of the 1kW Thermoelectric Generator for Diesel Engines. *American Institute of Physics*, 1995, 295-298.

7 **Ikoma, K., Munekiyo, M. and Furuya, K.** Thermoelectric Module and Generator for Gasoline Engine Vehicles. *17th International Conference on Thermoelectrics*1998).

8 **Hendricks, T.J. and Lustbader, J.A.** Advanced Thermolectric Power System Investigations for Light-Duty and Heavy Duty Applications Part 1&2. *International Conference on Thermoelectrics* (IEEE, Long Beach, CA, 2002).

9 **Crane, D.** Optimizing Thermoelectric Waste Heat Recovery from an Automotive Cooling System. *Mechanical Engineering* (University of Maryland, 2003).

10 **Headings, L., Marano, V. and Jaworski, C.** Opportunities for Thermoelectric Energy Conversion in Hybrid Vehicles. *ASME International Mechanical Engineering World Congress and Exposition*Chicago, Illinois, 2006).

11 **Incroprera, F.P. and Dewitt, D.P.** *Introduction to Heat Transfer*. (John Wiley & Sons, 2007).

12 **Lee, S. and Bae, C.** Effect of Design Parameters on the Performance of Finned Exhaust Heat Exchanger. *SAE International*, 2003, **2003-01-3076**.